Institut National Polytechnique de Grenoble- Phelma

Master in Micro and Nano technologies for integrated systems (MNIS)

Inertial MEMS sensors characterizations and design optimization

---

Student :

Felix Rodriguez Espinal

Felix-David.Rodriguez-Espinal@phelma.grenoble-inp.fr

Supervisor :

Ricciardi Carlo

carlo.ricciardi@polito.it

Tutor :

Panagiota Morfouli

liliana.prejbeanu@grenoble-inp.fr

Contents

List of Figures

1 Acknowledgement

I would like to express my gratitude to my advisor, Dr.Remi Robutel, for their unwavering support and guidance throughout my internship. His expertise and patience have been invaluable to me and have played a crucial role in the success of this thesis.

I am grateful to SLB for providing me with the opportunity to conduct my research and for all of the resources and support they provided me. I would like to extend a special thanks to Pierre Damery, who went above and beyond to help me with my manual work on the PCB.

I am deeply thankful to my friends and family for their love and support during this process. Their encouragement and motivation helped me to face the most difficult days.

I would also like to thank my colleagues at SLB for their support and collaboration during my research. In particular, I would like to thank Emmanuel Canivez for his help to find some specific equipment and for his assistance with the characterization of the MEMS.

Finally, I would like to extend my sincere gratitude to all of the participants in my study. Their willingness to share their experiences and insights has been invaluable to my research and has helped to make this thesis a success. Thank you for your time and contribution.

I am grateful to everyone who has supported me throughout this process. Without your help and guidance, this thesis would not have been possible.

2 Abbreviations

ASIC Application-Specific Integrated Circuit.

CEA Commissariat Energie Atomique (FR).

ESIP Environmental System-In-Package.

LETI Laboratoire d'Electronique et de Technologie de l'information (FR).

MEMS Micro Electro-Mechanical Systems.

NEMS Nano Electro-Mechanical Systems.

PCB Printed Circuit Board.

RMS Root Mean Square.

SNR signal-to-noise Ratio.

F.S. Full Scale.

ESD Electrostatic Sensitive Device.

DAQ Data Acquisition System.

R&D Research and Development.

FEM Finite Element Simulation.

SRPC SLB Riboud Production Center.

3 Introduction

Known as the biggest oil and gas services company worldwide, SLB provides state-of-the-art devices for the energy industry. Its reputation is due to the efforts that are put in R&D to do breakthrough innovation with each new device put into the market. 71 technology centers are present all around the world.

This internship has been carried out in SLB Clamart, also known as SLB Riboud Production Center (SRPC). It is a highly interdisciplinary center focused on standard and personalized tools for diagnostics during drilling [1]. It welcomes a large public from all over the world: research assistants, master's students, doctoral, and post-doctoral students, and subsidiaries. Among the last ones, there are some that work in other fields such as geothermal energy (e.g. Celsius energy) or hydrogen (e.g. Genvia). SLB Clamart is also a cosmopolitan place where you can learn a lot from other cultures. There are more than 1000 employees and 47 nationalities in this site.

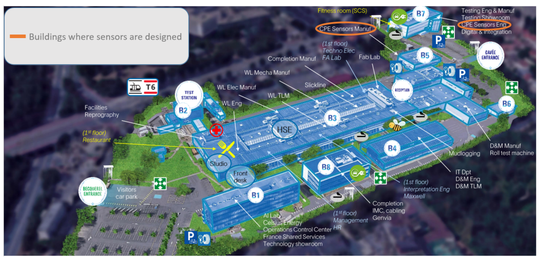

(a)

(b)

Figure 1: SLB SRPC. (a) Clamart site. (b) Entry.

Figure 2: Hierarchy electronics team.

Environmental System In Package (ESIP) is a project to develop a tiny sensor to be used in drilling rigs, in a harsh environment (pressure, temperature, humidity and shocks). The project consists of integrating a commercial humidity and temperature sensor with a 4-axis MEMS transducer (3-axis accelerometer and a pressure sensor).

Very often, Micro Electro-Mechanical Systems (MEMS) inertial sensors are based on a suspended proof mass that will move according to an external perturbation. The movement can be detected by a change in the capacitance between two films, by a change in the voltage of a piezoelectric material, or even by a change of the resistivity, thus a change of the resistance, of a piezoresistive material.

The project uses a piezoresistive MEMS sensor that was patented by the CEA-Leti. The main innovation lies in the size of the proof mass and the piezoresistive gauges that improve the sensor's performance (nanogauges are active resistive elements, resulting in a readout mechanism less dependent on temperature and with a better sensitivity), low unit cost (at high volume) and reduce its overall footprint (the sensors follow a complex but controlled process that allows designing a 3-axes accelerometer on the same silicon chip). Besides, the MEMS has an embedded self-test that can be used for calibration and sensitivity evaluation, at a lower cost. The current report will focus on the accelerator part and particularly on its characterization in order to obtain an empiric model of comparison. To perform experiments with the accelerometers of a given MEMS (3 acceleromete s/axis inside one MEMS) a larger PCB has been designed (MEMF001 see section 5.6) to adapt the outcoming signal of the MEMS, to the requirements of the project (filtering, amplification and offset regulation).

4 Theoretical background

In this section a summary of the main effects present during the design project will be shown.

4.1 Piezoresistive effect

Piezoresistivity is a complex phenomenon to understand in detail. But in a few words, it describes the fact that some materials are able to modify, mainly, their electrical resistivity according to mechanical stress or strain that is applied externally to the nanogauge (in the case of the inertial MEMS used in this project) [3]. It allows to convert a mechanical perturbation or force into an electrical signal.
Let's take a semiconductor of length L (m), of electrical resistivity $\rho(\Omega.m)$ and area $A(m^2)$. The formula of the resistance $R(\Omega)$ can be extracted using the following formula:

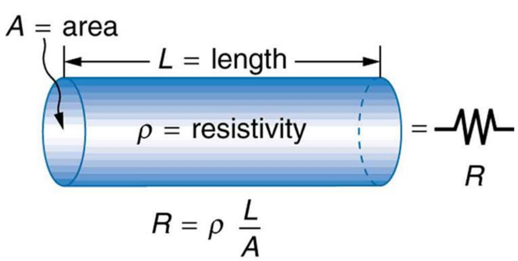

(a)

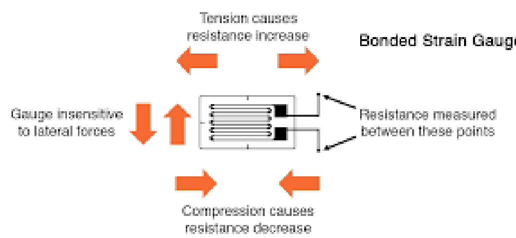

(b)

Figure 3: (a) formula of the electric resistance according to the resistivity of the material. (b) Resistance change under axial or compressing stress.

4.2 Thermal sensitivity (TCR)

In the previous part, it has been shown that the nanogauge electrical resistivity, thus the electrical resistance, depends on the mechanical stress. However, it is not the only parameter to take into account, there is also the temperature variation. This last parameter can be detrimental to the sensitivity of the sensor and it could increase the offset at the output. The CEA-Leti has studied this dependence during the design [2] and found a linear relation between -40°c and 175°c with a temperature coefficient of resistance (TCR) of 1400ppm/K approximately.

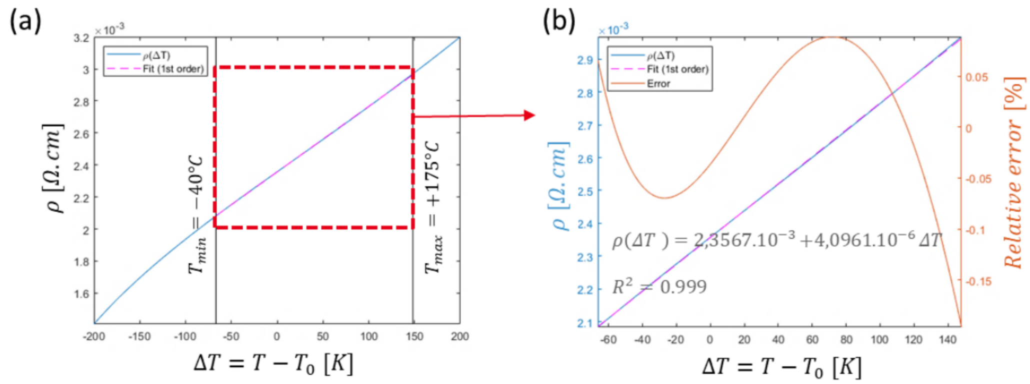

Figure 4: (a) Electrical resistivity dependence with temperature within [-40°C, +175°C] range for p-type silicon doped with Boron at 5.10^{19} at/cm3 and (b) linear fit used to extract the related temperature coefficient of resistivity. Both figures are extracted from [2].

4.3 Self-heating

Even though self-heating effect happens inside the MEMS sensor and this part is not done during the internship, self-heating could affect the resistivity and consequently the output signal of the gauge.

The higher is polarization voltage of the Wheatstone bridge, the better will be the signal-to-noise ratio. However, the joule effect will also increase self-heating. If this effect is taken into account, the output signal will not be linear with respect to the resistivity anymore.

According to a previous study, the maximum self-heating temperature allowed should be 100°c [4].

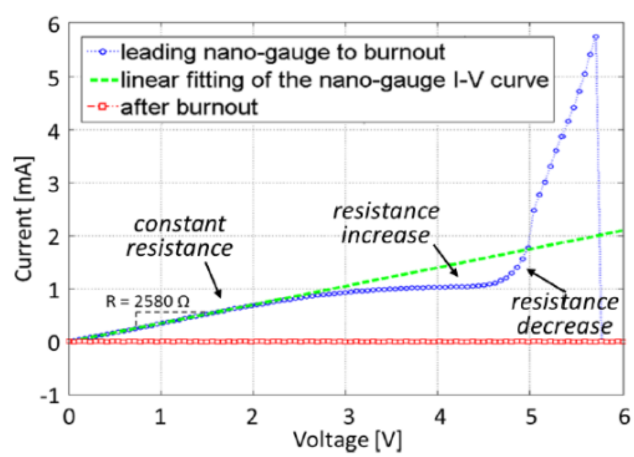

Figure 5: Current to voltage (I-V) experimental curve of a 2.58 KΩ. N&MEMS piezoresistive nanogauge under increasing biasing current. The electrical resistance remains constant up to a current of 900uA then starts to increase slightly (likely due to a decrease in carrier mobility) before rapidly decreasing (due to an increase in carrier concentration by thermal generation) and leading to failure. Figure are extracted from [2].

4.4 Electrical noise sources

The two main noises that could disturb the signal are the thermal and the flicker noise (also mechanical noise could occur but it is considered negligible). The thermal noise limits the maximal resolution, whereas flicker noise is present at low frequencies or long observation times.

The thermal noise is a white noise (constant noise) caused by induced agitation of the electrons (in this case) inside a resistive object. The equivalent noise voltage can be computed from the power spectral density over the bandwidth as follows:

$$e_{TH,RMS} = \sqrt{4K_BTR(f_{max} - f_{min})} \tag{1}$$

K_B stands for the Boltzmann constant(J/K), T the operating temperature(K), R the electrical resistance(Ω) and f_{max}-f_{min} is the bandwidth(Hz).

The flicker noise is a noise that will reflect the imperfections inside the silicon lattice of the piezomaterial. There is a 1/f dependence on the power spectral density [5]. The equivalent noise voltage can be computed as follows:

$$e_{FL,RMS} = V_{bias}\sqrt{\frac{\alpha_H}{N_{dop}V_{gau}}ln(\frac{f_{max}}{f_{min}})} \tag{2}$$

V_{bias} stands for the applied bias voltage(V) to one gauge (i.e. $V_{bias} = 0.5V_{pol}$), α_H=2.10^{-5} for the Hooge constant, N_{dop} for the doping concentration (at/m^3) and V_{gau} for the nanogauge volume (m^3).

The overall signal-to-noise ratio is [2]:

$$\frac{1}{SNR^2} = \frac{1}{SNR^2_{TH}} + \frac{1}{SNR^2_{FL}} \tag{3}$$

4.5 The 3-axis accelerometer

The MEMS sensor is composed of a pressure sensor and a 3-axis accelerometer. As it was said before, during the internship only the 3-axis accelerometer is studied. Its structure allows the detection of a force or an acceleration in any direction in space. 2 axes are used to detect in-plane accelerations and they have the same design. The last axis is designed differently in order to detect out-of-plane accelerations in the same chip.

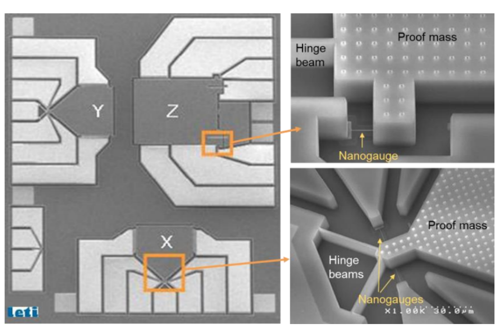

Figure 6: SEM pictures of MEMS 3-axis accelerometer with close-up views on mechanical elements. Figure extracted from [2].

Even though, the axes have not the same design, they operate on the same principle. For full bridge configuration,two transducers, as in figure called ***SEM pictures of MEMS 3-AXIS accelerator with close-up views on mechanical elements.***, are coupled. An input acceleration will turn the proof mass and create a mechanical stress within the nanogauges. One gauge will be compressed whereas the second one will be stretched. The difference of mechanical stress will change the overall resistivity and, thanks to the piezoelectric properties of silicon, the electrical resistance can be calculated. The principle is detailed in the figure called ***Simplified schemes of MEMS accelerometer working principle in-plane axis.***

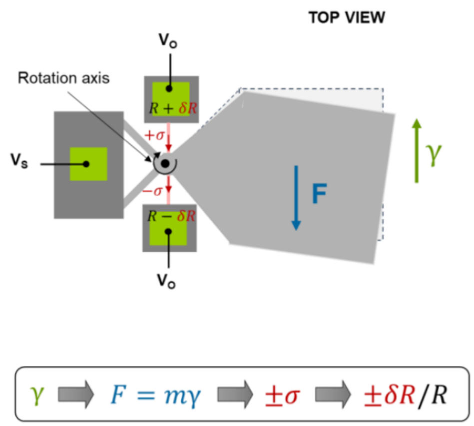

Figure 7: Simplified schemes of MEMS accelerometer working principle in-plane axis.Figure extracted from [2].

4.6 Nanogauge readout mechanism

From an electrical point of view, only the nanogauges seem to contribute a change in the resistance. As the proof mass is not polarized, the equivalent electrical model of an accelerometer can be represented as two resistors in parallel, each resistor being the resistance of a nanogauge. Heavy doping of silicon is used to make gauges piezoresistive, but also for electrical routing through the device. The main advantage is that nanogauges are active resistive elements, resulting in a readout mechanism less dependent in temperature and with a better sensitivity.

By doing a Wheatstone configuration, as the figure called ***Wheatstone bridge approximation of the X1 axis.*** a change in the resistance can be measured precisely as a change in the output voltage according to the following formula:

$$V_{out} = \left(\frac{R_3}{R_3 + R_4} - \frac{R_2}{R_2 + R_1}\right)V_{pol} \tag{4}$$

If it is assumed that at equilibrium all the nanogauges have the same resistance, the condition $\frac{R_1}{R_2} = \frac{R_4}{R_3}$ is fulfilled and the output voltage will be null. When an acceleration is detected, there is a change in the resistance of the nanogauges. If the nanogauges pair are strategically placed in the wheatstone bridge, a linear behaviour between the resistance variation and the output voltage can be found. The last equation can be rewritten as:

$$V_{out} = \left(\frac{R + \Delta R}{R + R} - \frac{R - \Delta R}{R + R}\right)V_{pol} = \frac{\Delta R}{R}V_{pol} \tag{5}$$

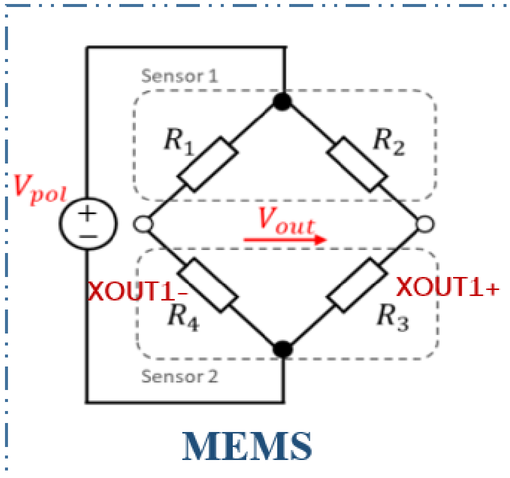

Figure 8: Wheatstone bridge approximation of the X1 axis.

4.7 Extra features

self-test mechanism is built next to the accelerometer in order to create an autotest inside the MEMS accelerometer (It allows to simulate accelerations up to 1000 g). Stoppers are designed for survivality shocks [7].
The electrostatic actuator is different for in-plane or out-of-plane axis. In the first case, it has inter-digitized fingers that are designed to provide a consistent gap actuation, the principle is shown in the figure called ***In-plane axis gauge stress and mass displacement under electrostatic actuation.***. It can be split into two main parts: a stator (fixed) and a rotor (attached to the proof mass). When a voltage is applied between the two parts, the electrostatic force will bring near the two parts thus increasing the electrical capacitance. The second case works under the same principle but without using inter-digitized fingers and thus it is vulnerable to the snap-in phenomenon that limits the displacement to one-third of the gap, the principle is show in the figure called ***Out-of-plane axis electrostatic actuation module configuration and geometry.***. Previous simulations [2] have shown that this effect can be neglected for an applied voltage lower than 17V. It must be confirmed by carrying out experiments.

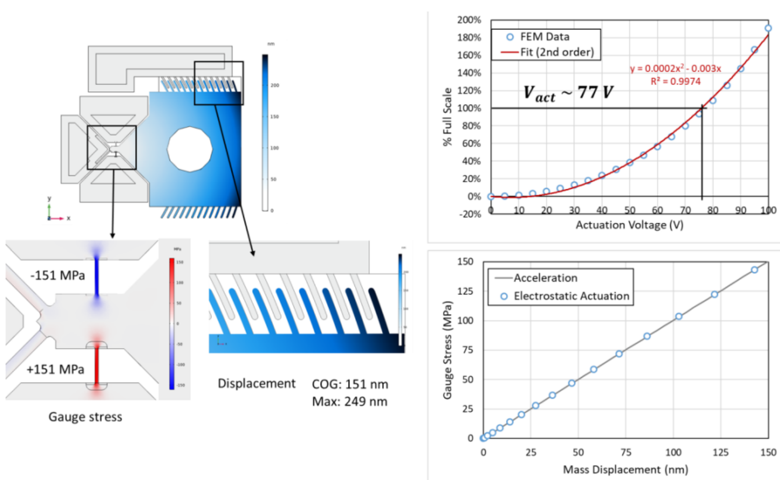

Figure 9: In-plane axis gauge stress and mass displacement under electrostatic actuation.

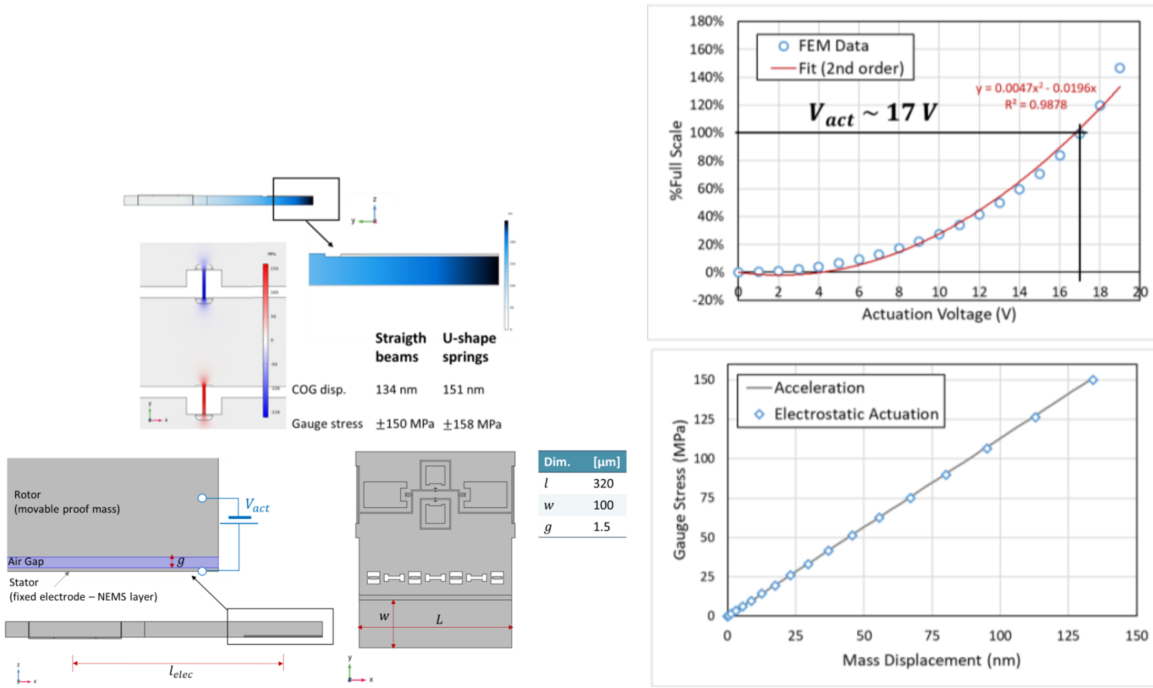

(a) (b)

Figure 10: (a) Out-of-plane axis electrostatic actuation module configuration and geometry. (b) Out-of-plane axis FEM simulation results of a straight beam.

5 Statement of the project

As it was explained during the introduction, the goal at the end is to characterize the MEMS in order to confirm its behaviour and extract an empiric model that will be compared with simulations. To main concern at the beginning of the internship was the design of the PCB to filter, amplify and reduce the offset signal at the output of several accelerometers at the same time. Since several sensors will have the same configuration, the circuit must be compacted and scalable. The requirements are:

- Cutoff frequencies of f_{c1}=1 Hz and $f_{c2}>$ 50KHz.
- Amplification quite high avoiding saturation (1% of accuracy).
- Offset lower than 30% of the Full-Scale (F.S) value.

Concerning the last requirement, to have an order of magnitude. Let's suppose that the polarization voltage is V_{pol}=400mV and that the sensitivity of the accelerometer is around 50µV/V/g and the maximal acceleration allowed is a_{max}=1000g (1g=9.80665m.s^{-2} the letter g will be used all along the report. It will always correspond to an acceleration). The resulting Full Scale is:

$$F.S. = sensitivity.V_{pol}.a_{max} = 20mV \tag{6}$$

Therefore the offset voltage cannot be higher than 30% of the F.S. which is around 6mV in this case. The criteria of 30% off the full scale is a trade off. More details will be given at 5.1.2 section.

5.1 Sizing of the circuit

In this section the different stages for filtering, amplification and offset will be sized.

5.1.1 Filtering

To fulfill this function without affecting the rest of the circuit and keeping it compact, the simplest idea was to use an active pass band filter. The main advantage is that the gain of the filter is more stable and independent from the rest of the circuit. The transfer function of the filter can be written as:

$$T_{filter} = -\frac{R_2}{R_1} . \frac{1}{1+\frac{j\omega}{\omega_2}} . \frac{\frac{j\omega}{\omega_1}}{1+\frac{j\omega}{\omega_1}} \tag{7}$$

Where ω_1 and ω_2 are the pulsations that are linked by the following equation: $\omega_1 = 2\pi f_{c1} = \frac{2\pi}{R_1 C_1}$ and $\omega_2 = 2\pi f_{c2} = \frac{2\pi}{R_2 C_2}$. To facilitate the next steps the filter will have a unitary gain (-1). Therefore, R_2=R_1

5.1.2 Amplification and offset

The outcoming signal of the MEMS accelerometer has an amplitude roughly of 20mV. Knowing that the output signal must be kept between the range [-10V,+10V] (input range of the DAQ) and that the filtering stage has a unitary gain, the proposed configurations have been adapted to the gain of the project. Therefore, an external resistor Rg, has been used to fix the theoretical gain at 452.1. The circuit on the figure called ***Automatic DC restoration using an external resistor Rg in LT-Spice.*** has been tested on the breadboard (LT-Spice is only used here to illustrate the circuit):

The datasheet of the instrumental amplifier INA103KP [8] has a basic circuit configuration that allows to select the gain. It is very useful to easily modify the gain of the whole circuit. Moreover, there is also a configuration for the automatic DC restoration that can be helpful.

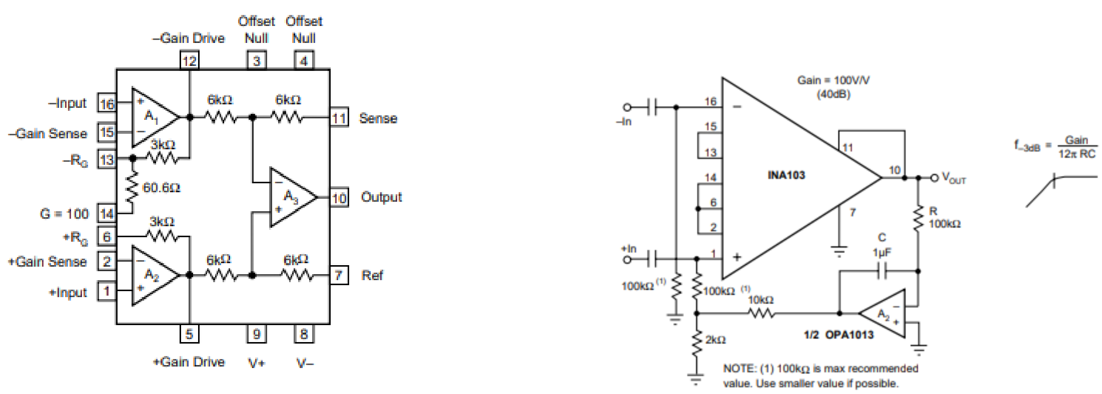

(a) (b)

Figure 11: (a) Connections of the instrumental amplifier INA103KP (b) Automatic DC restoration proposed in the datasheet [8].

The main advantage of that circuit was the fact that the offset value was set automatically without intervention. Some tests were made at the beginning but the offset was often larger than 30% of the full scale, when the full circuit with the other stages was tested. Indeed, this last requirement represents the dispersion of the sensitivity

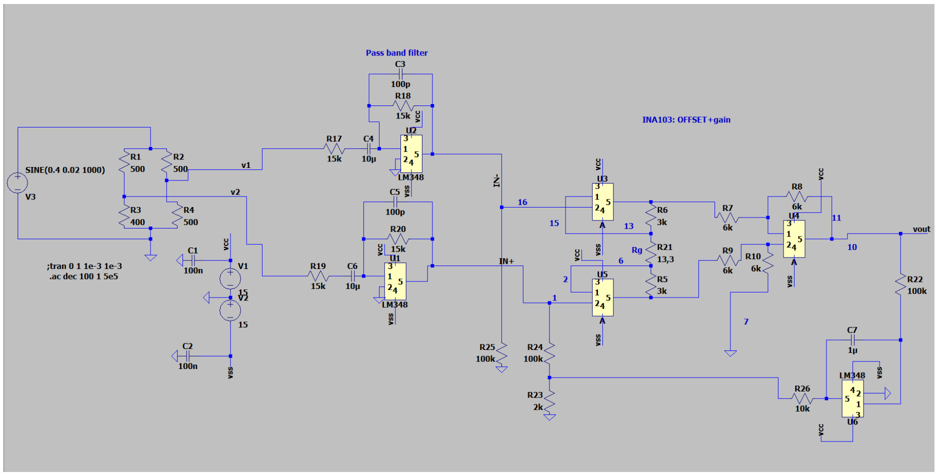

Figure 12: Automatic DC restoration using an external resistor Rg in LT-Spice

of the MEMS accelerometer. If a larger dispersion is allowed, more MEMS accelerometers would match the offset requirement but the high gain of the amplification stage will saturate the signals of some of those MEMS. In the other way, if the a better accuracy is demanded, the number of MEMS that would be disposed becomes too important. Therefore, a trade-off is found at this value and this requirement cannot be modified. Another circuit has been tested using potentiometers:

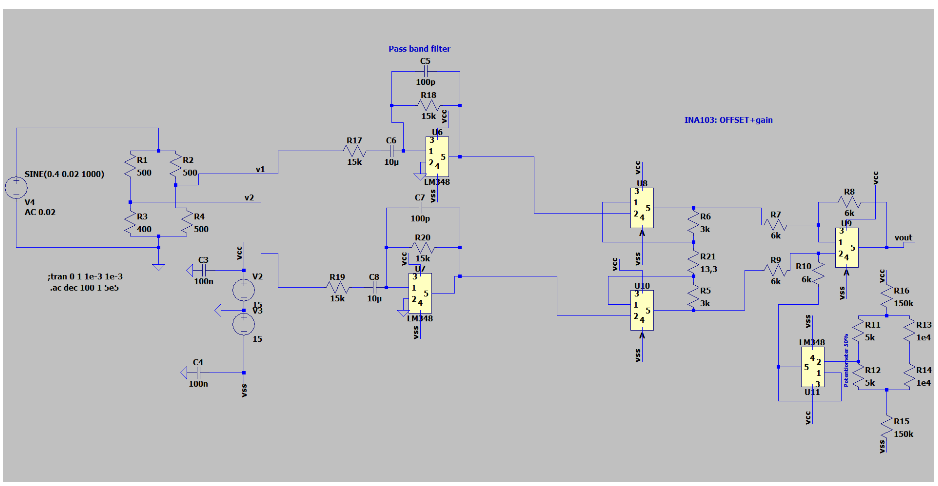

Figure 13: DC restoration using potentiometers.

This configuration has been tested on the breadboard with the other stages of the circuit and it works perfectly. The output was fixed between [-9.05V,+9.05V] (according to the sensitivity of each MEMS) to let some margin with the full scale and be sure that the circuit will not saturate. The instrumental amplifier allows to set of the gain using only one external resistor that can be changed later to get closer values to the full scale. For the design, only this external resistor was set to 0.1% accuracy to reach the goal of 1% accuracy of the PCB. Later on, it will be shown that other passive components should have the same accuracy to achieve this goal.

5.2 Transfer function

The next step was to plot the Bode diagram in order to find the experimental transfer function of the circuit and to confirm that there is no perturbation between the MEMS (that is represented by the Wheatstone bridge circuit), the filtering circuit and the instrumental amplifier. The last part represents the amplification stage and it will only shift the Bode diagram vertically (the gain of the transfer function will be different but the cutoff frequencies will remain the same)

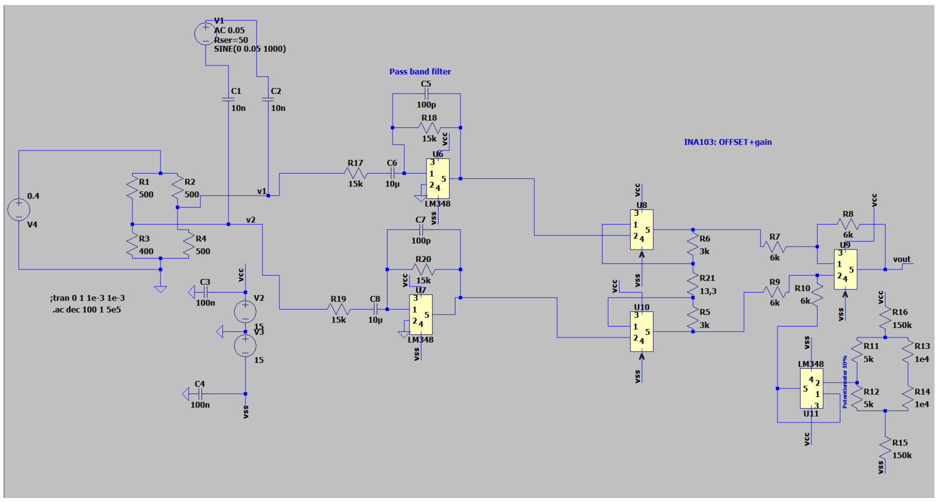

Figure 14: figure of the connections of the real circuit. AC signals are inserted using an oscilloscope put in parallel with respect to the circuit.

To add a sinusoidal signal, an oscilloscope has been put in parallel to the Wheatstone bridge. The oscilloscope has an output resistance of 50Ω. Two capacitors were put between the oscilloscope and the Wheatstone bridge to avoid noise coming from the oscilloscope.

There is no difference between the filtering and the whole circuit. It has a higher gain because of the amplification stage, but there is not a shift in the frequency. However, the capacitors put between the oscilloscope and the Wheatstone bridge play a role in shifting the cutoff frequency f_{c1} of the whole circuit.

Indeed, the capacitors used to split the oscilloscope from the Wheatstone bridge also form a high pass filter. Both capacitors are in series with the series resistance of the oscilloscope and the equivalent resistance of the Wheatstone bridge. Hopefully, the capacitors are only used to inject an AC signal to plot the Bode diagram, they do not belong to the real circuit. Therefore, if very high capacitance values are used the cutoff frequency will be very low and the effect of the coupling capacitors will be neglected.

Thanks to the Bode diagram, the transfer function can be found. If the oscilloscope and the capacitors, used to split it from the rest of the circuit, are not taken into account and only the original circuit, the gain, and the cutoff frequencies are easily shown and the transfer function can be calculated:

$$T_{circuit} = -\frac{R_2}{R_1}.\frac{1}{1+\frac{j\omega}{\omega_2}}.\frac{\frac{j\omega}{\omega_1}}{1+\frac{j\omega}{\omega_1}}.K \approx \frac{-452.128}{(1+jf)(1+\frac{jf}{10^5})} \tag{8}$$

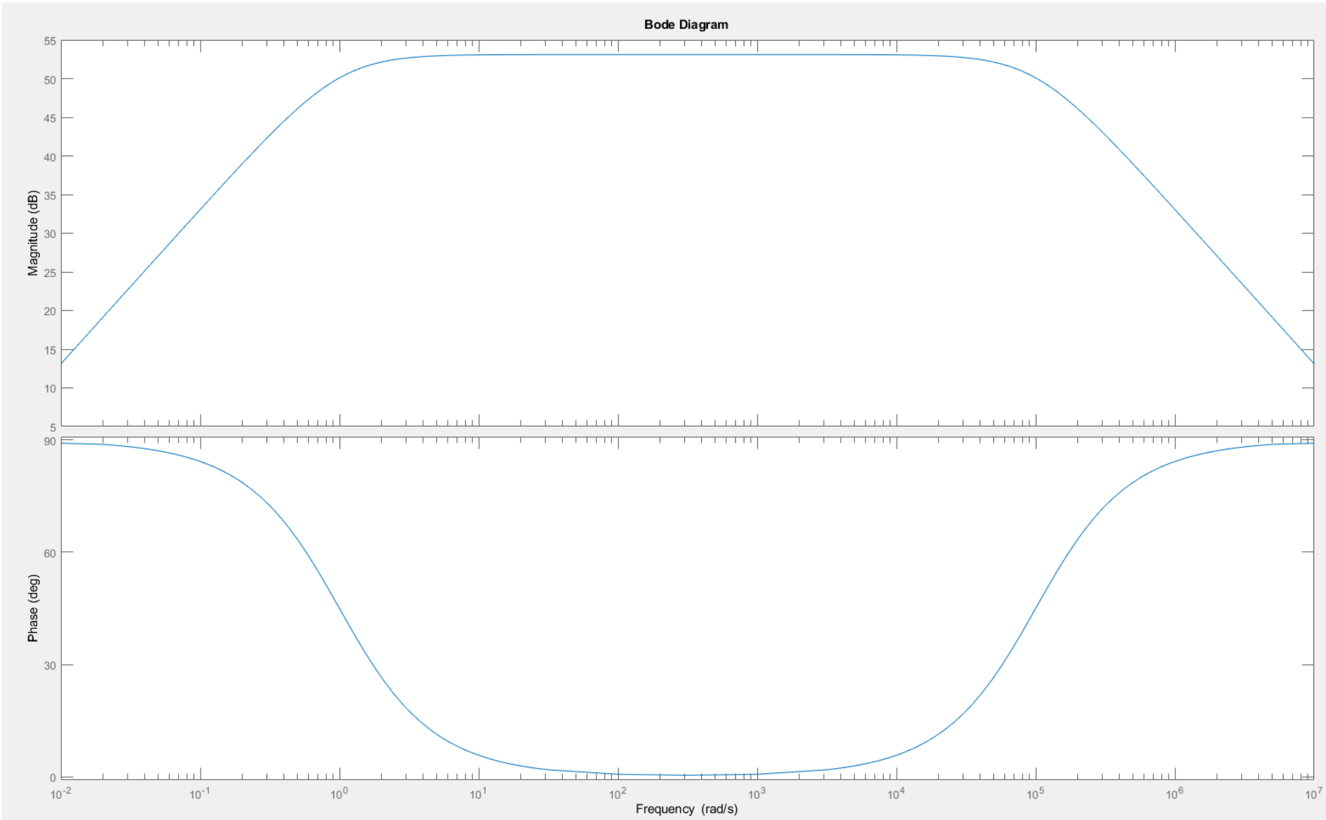

Figure 15: Theoretical Bode diagram.

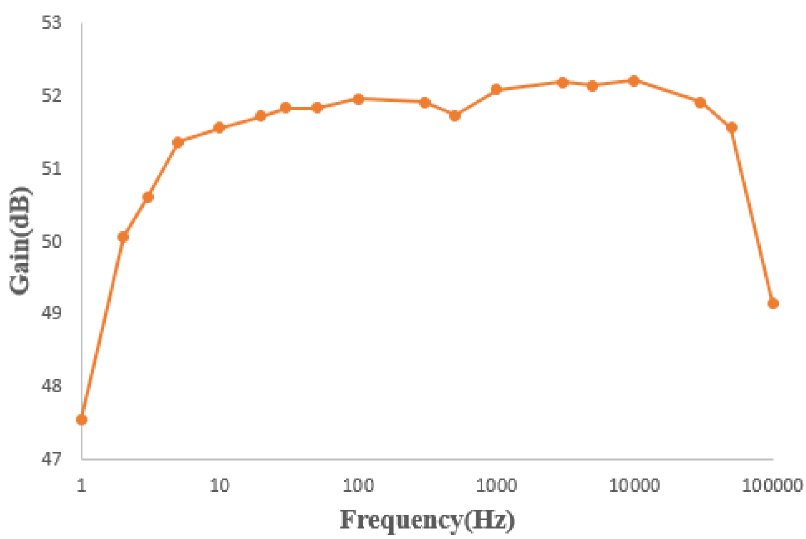

Figure 16: Experimental Bode diagram. The bandwidth fits with the requirements.

5.3 Step response

It seems that there is not a minimum voltage at the input to have a stable response. The amortized behavior can be confirmed. It is an over-damped system. The system is a second order, that can be approximated by a

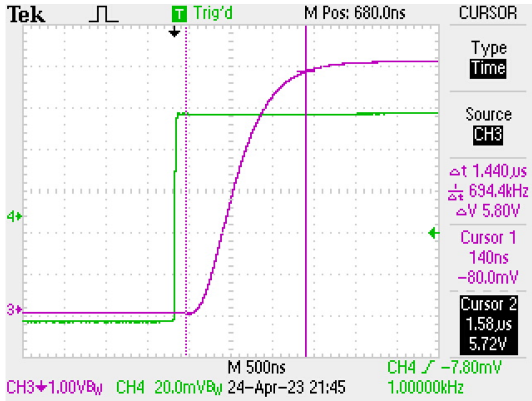

Figure 17: picture of the step response taken from the oscilloscope.

first-order far from t=0s. Consequently, 3τ can be approximated as the latest time to reach 95% of the final value. In this case 3τ=1.44us. It allows a fast and stable amplification circuit for the project. It suits very well.

5.4 Allan deviation

The Allan deviation is one of the most iconic charts of MEMS/NEMS and in particular gyroscopes and accelerometers. It allows us to show the different kinds of noises present in a device. It is done by measuring N samples divided into k groups of n samples. The groups can overlap each other [9]. If the group averages are computed, the

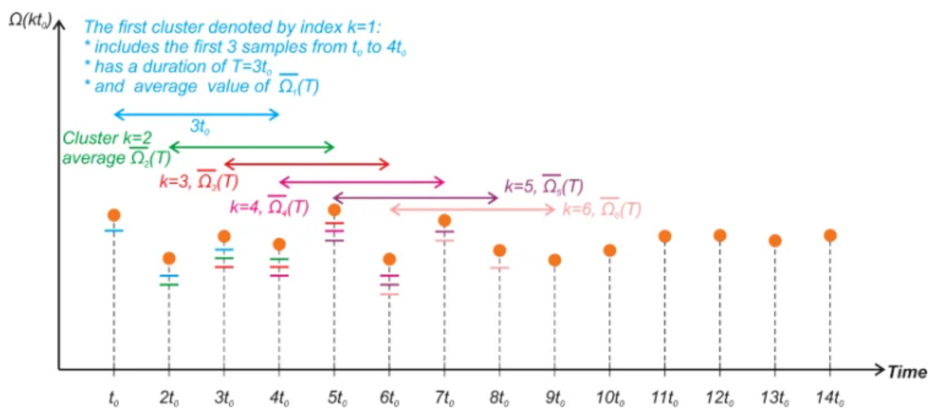

Figure 18: overlapping Allan variance

Allan variance can be computed using the formula:

$$\sigma^2(T) = \frac{1}{2(N-2n+1)} \sum_{k=1}^{N-2n+1} \left(\overline{\Omega}_{k+n}(T) - \overline{\Omega}_k(T)\right)^2$$

Figure 19: Overlapping Allan variance formula.

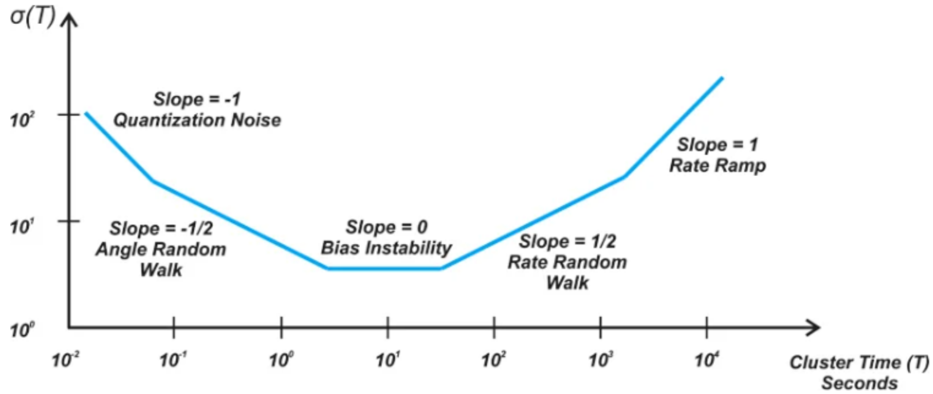

Figure 20: Expected Allan deviation plot.

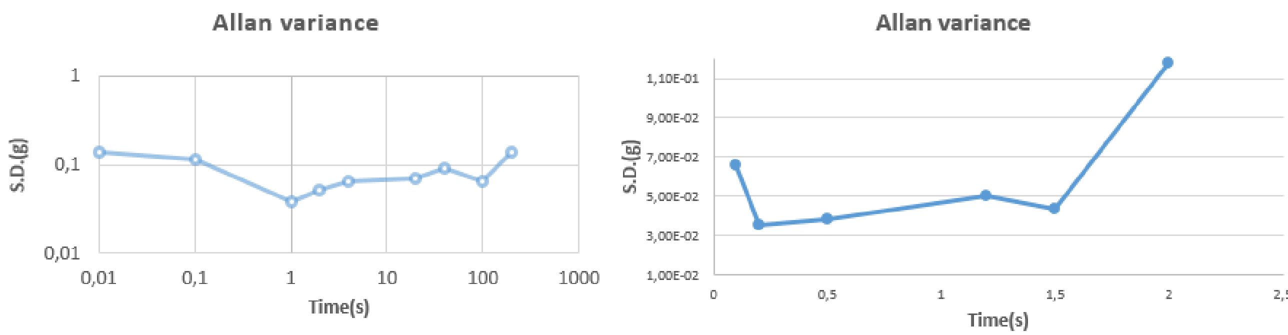

Figure 21: (a) Allan deviation plot of the circuit before designing the PCB MEMF001. (b) Allan deviation plot obtained using all the setup. The measurements were done between 0.1s and 2s to have an accurate value of the minimum.

The plot does have the similar appearance as the theoretical curve. The minimal step(maximal resolution) found in this case is 0.0039g.

5.5 Reference sensor

In order to compare the obtained data with a calibrated accelerometer, that will be the reference, the idea was to design a circuit (a charge amplifier using an integrator stage) to amplify the signal to the same amplitude as the inertial MEMS. A circuit from Texas Instruments was found [10] using the same bandwidth but the component wasn't available. Therefore, the test should be done using a similar component. To replace an amplifier several criteria were important, such as the voltage range, the power supply requirements, the noise, the gain bandwidth, and the bias current. Some time has been lost because the circuit didn't work. Indeed, the component used for the test had a bias current much bigger than the one proposed by the circuit of Texas Instruments. To ensure the delivery of the PCB soon enough for the tests, the decision was to use the same components of the circuit proposed by Texas Instruments in the PCB design. However, when the PCB was received the circuit was functional but the the Full scale was a bit different than the one of the channels.

5.6 PCB design

Once the circuit has been entirely tested and simulated, the next step is to design it in a PCB for manufacturing. The goal at the end is to be able to test several MEMS at the same time. Consequently, several PCB are required. The choice was to focus on the design, to make a design easy to reproduce, with few layers and compact but well organized, and to ask an external manufacturer for the production and be sure that it would be made on time. Eagle was the software used for the design of the PCB. It was very intuitive and easy to learn (thanks to other design software used during the master).

No serious problem was found in designing it. However, some manual modifications were necessary after it was delivered, in order to carry out all the experiments. Furthermore, additional precaution has been taken in comparison with previous steps as a considerable amount of money has been invested in the PCBs.

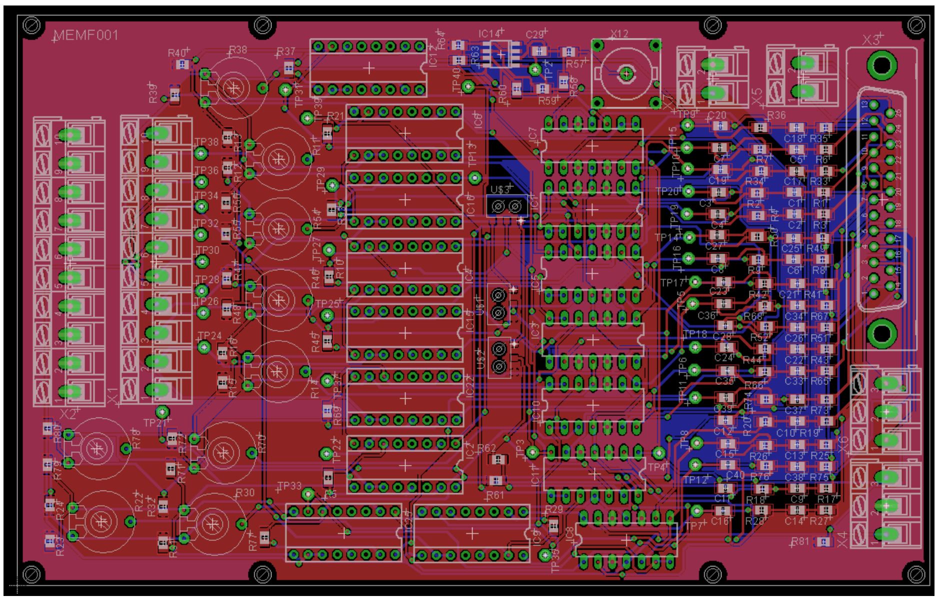

Figure 22: Design of the PCB in Eagle.

6 Steps to carry out an experiment

In this section, all the steps from the setup to the acquisition will be explained in detail. Even if the microfabrication process fits very well with the master's content, it will not be discussed in this report because it wasn't the main point of the internship. However, microfabrication was very important at the beginning of the internship to understand the inertial MEMS' functionality.

6.1 Equipment and experimental setup

In order to perform the experiments, the tools that are used include:

- An oscilloscope for the visualization of the signals.
- A multi-meter for accurate measurement.
- A breadboard to test different circuit configurations.
- Operational amplifiers used in the filtering and offset regulation stages [11].

(a) (b) (c)

Figure 23: (a) Tektroniks DPO2014B Oscilloscope (b) Keysight U1231A Multi-meter (c) Breadboard.

- Instrumental amplifiers for the amplification and offset regulation stages [8].
- A voltage source for all the components of the PCB and for the self-test.

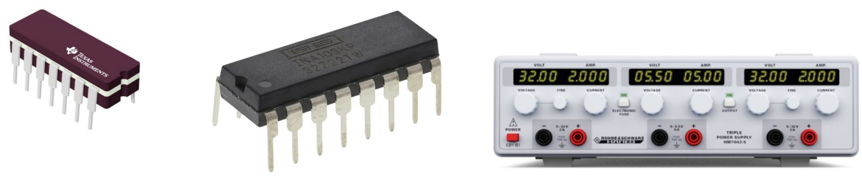

(a) (b) (c)

Figure 24: (a) LM238n Operational amplifier (b) Instrumental amplifier INA103KP (c) HAMEG HM7042-5 Voltage source.

- A low frequency generator to simulate a shock wave.
- Inertial MEMS to be characterized.
- A current source to polarize the Inertial MEMS.

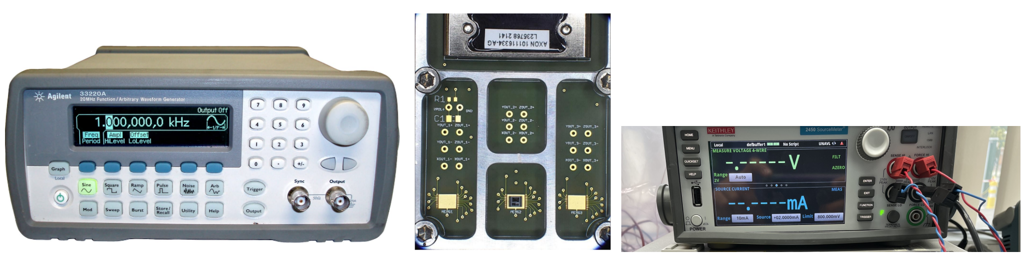

(a) (b) (c)

Figure 25: (a) Agilent 3322A low-frequency generator (b) Inertial MEMS (c) Keithley 2450 source meter. It was used as a current source for the experiments.

- Resistors welded in the PCB.
- Capacitors used for the active filter design.
- DAQ to digitize all the data in parallel.

- A computer for the visualization and the recording of data.

At the beginning of the internship, different kinds of circuits concerning the filtering stage and amplification stage were tested on the breadboard (see figure called ***LTspice simulation of the whole circuit.***). Transversal components were used and placed on the breadboard according to the configuration. Then, the whole circuit was tested before starting the design.

As soon as the PCB arrived (the acquisition board), it was possible to put all the setup together. It has three main parts: the MEMS that has a current source as an input, it generates a polarization voltage at the output together with the acceleration signals of each axis (as a difference of electric potential), the PCB MEMF001 that will filter, amplify and regulate the offset, and finally the DAQ system with the computer to digitize all the data recorded.

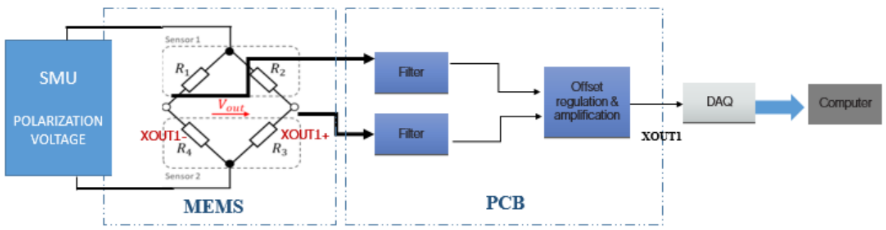

Figure 26: Simplified representation of the setup

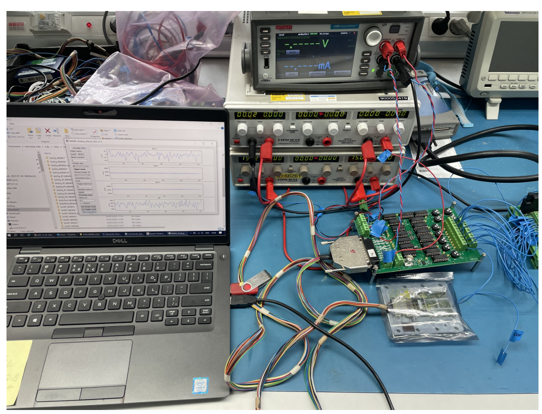

Figure 27: All the setup

To carry out an experiment, ESD protection is used. First, the current source is activated at 3-4 mA. The polarization voltage value is observed and if it is not between 0.3 V and 0.5 V, the current source value is modified. If those values are incompatible with a MEMS, it already gives an idea of the sensitivity of the sensor (it would be far from the ideal value of 50 uV/V/g).

The next step is to activate the voltage sources (first the voltage source of the power supply for the amplifiers is activated and after the other voltage source is activated either to test a channel without using the MEMS or to carry out the self-test). It is mainly done as a precaution to avoid harm to the MEMS devices because they are very fragile. To turn off the devices the procedure is done in the opposite way.

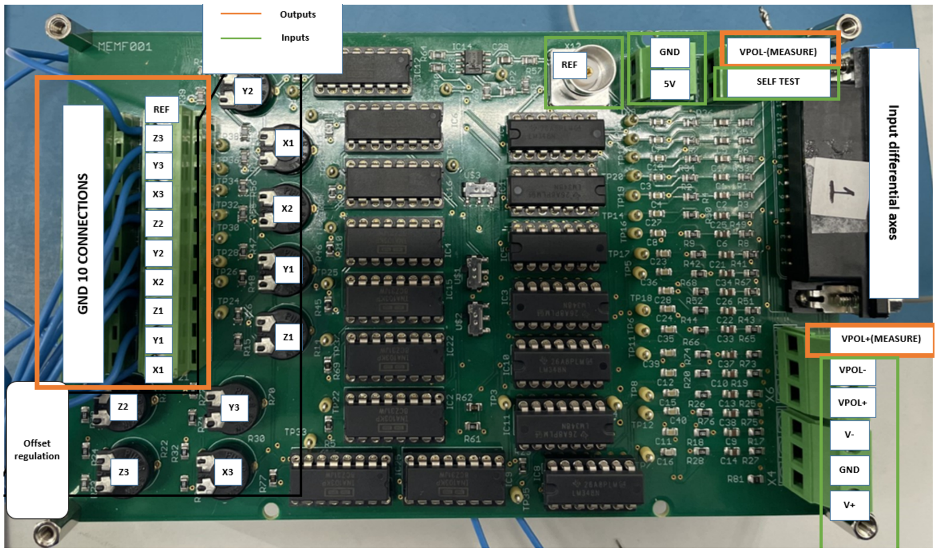

Figure 28: PCB labeled

6.2 Data processing and analysis

Once the setup is ready, an AC study, a DC study, or a shock study in the vibrator test bench can be performed. The DAQ has some constraints: the output is limited to ± 10 V, the sampling rate is 250K Samples/s for one channel maximum and the trigger was only able to record data after the peak of a shock.

The output range limitation only fixed the gain of the amplification stage of the PCB, consequently it was not a big problem. The sampling rate could be detrimental to the data if the sampling frequency per channel is not high enough, but some tests have shown that the sampling rate of the DAQ is enough for a shock. indeed the shock can be approximated by a half-sine profile in the time-domain with a period within 1.3 to 10 ms [13].

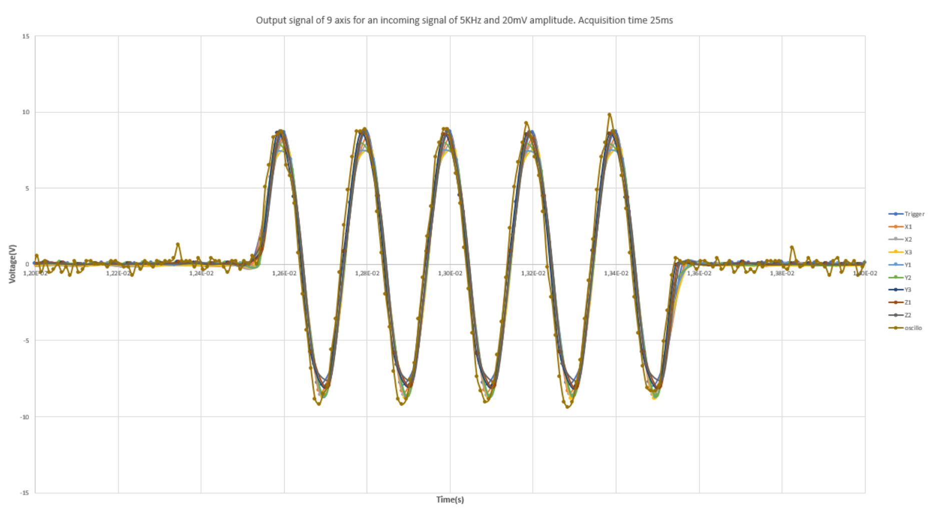

Figure 29: Test recording 10 channels at high frequency (compared to a shock wave) and at maximum output swing. It allows us to see the limits of resolution of the DAQ.

In the real setup also ten channels are used (nine axes and the reference sensor). The sampling rate is, in that case, 25K Samples/s. In order to record data before the shock, the trigger mode has been changed to another of the pre-defined modes. The middle trigger is a trigger mode that sets the trigger in the middle of the data record. It is the only trigger mode that records before the shock (among the three modes proposed in the data-sheet of the DAQ) [6].

The DAQ has a 16 bit resolution. Therefore, the output values of the DAQ are between -32768 and 32767. To convert the data into a voltage the following formula is used:

$$V_{out} = \frac{output.2^{bits}}{Range} \tag{9}$$

7 Characterization and results

In this section all the studies that were carried out will be shown and explained. 5 identical PCBs (MEMF001 model) were manufactured and during the section they will be named from PCB1 to PCB5.

7.1 AC study

The AC study has been done without an inertial MEMS. A low-frequency generator was used and connected to the differential inputs of the PCB. The input was a sinusoidal signal of f=1KHz and an amplitude of 20mV.

7.1.1 Bode diagram

To confirm the designed bandwidth, the gain of each channel must be measured at several frequencies. As this process is a bit tedious, it was only made on one PCB. The measurements showed that the bandwidth is correct.

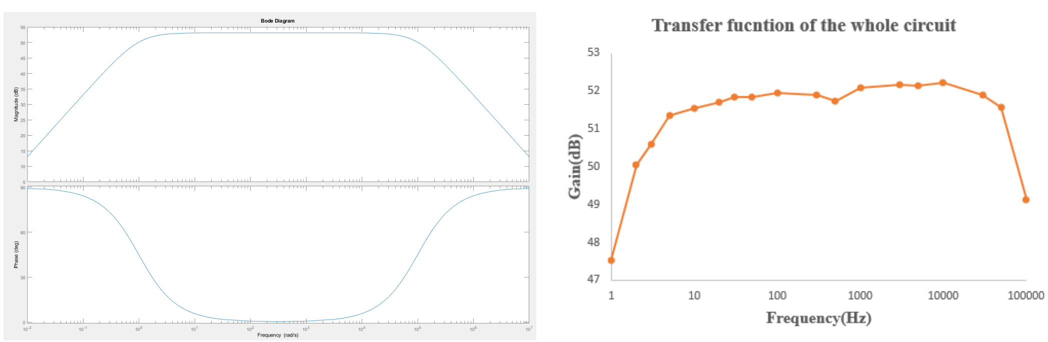

(a) (b)

Figure 30: (a) Simulated Bode diagram on Matlab. (b) Bode diagram of the designed PCB.

7.1.2 PCB's gain accuracy

As the gain accuracy is one of the three main requirements of the project, measurements of each channel of each PCB were made at a given frequency (f=1KHz). Indeed, the standard deviation of the gain measurement was higher than expected (3σ higher than 1%) because only the resistor that fixes the gain was designed for an accuracy below 1%. For instance, all the capacitors used for the active filter have an accuracy higher than 1% (5% and 10% respectively).

	AC CARDS			DC CARDS		F=1KHz			F=100Hz		
Axis	PCB#1	PCB#2	PCB#3	PCB#4	PCB#5	PCB#1	PCB#2	PCB#3	PCB#4	PCB#5	Theoretical gain
X1	452,1224	452,3692	449,5933	449,6677	445,6654	0,004957	0,059544	0,554458	0,537993	1,423259	452,1
Y1	449,6181	450,6417	451,4539	449,4465	446,7564	0,548964	0,322571	0,142907	0,586929	1,181945	3σ AC cards (%)
Z1	449,6925	448,2504	447,9783	449,2255	447,1624	0,532516	0,8515	0,911678	0,635817	1,092142	1,095183875
X2	448,8692	452,5223	449,0399	449,7537	448,4536	0,714616	0,093399	0,676868	0,518979	0,806545	3σ DC cards (%)
Y2	451,9941	449,4465	449,9013	449,2255	446,5378	0,023426	0,586929	0,486334	0,635817	1,230302	1,018152295
Z2	451,3667	447,8859	449,4293	450,209	446,1012	0,162208	0,932108	0,590742	0,41827	1,326875	3σ All cards (%)
X3	450,5657	451,1776	447,9705	446,4242	447,8783	0,339379	0,20402	0,913409	1,255427	0,933789	1,228138235
Y3	452,2576	448,4283	446,4067	445,6628	446,4548	0,034857	0,812145	1,259307	1,423851	1,248669	
Z3	447,7539	447,2387	448,3436	447,6957	446,8085	0,961312	1,07528	0,830887	0,974191	1,170425	
	Gains					Error percentage					

Figure 31: Gain of each channel of the 5 PCB and its standard deviation in %.

7.2 DC study

The AC study allowed to verify the bandwidth of the intended filter. However, the functionalities are limited. For instance, the filters cut the DC component of the signal and the offset of the MEMS can not be measured, the small variations can not be seen and the sensitivity can not be calculated. That is why pass-band filters were removed from two PCB cards to perform the DC study (PCB4 and PCB5). The goal would be to be able to measure the sensibility with a 5% accuracy. Less than 10% would be acceptable. As this requirement is not sure to be reached, two methods were selected to measure the sensitivity: the self-test and the ± 1g F.S. measurement method. If none of the methods can guarantee less than 10% accuracy, it means that each MEMS should be calibrated manually and it would considerably increase the cost price of the inertial MEMS 3-axis that has been chosen for the project. The shown data correspond to the characterization of the new MEMS. DC study was carried out also on old MEMS but they are less robust (the data is available in the Appendix).

7.2.1 MEMS' Offset

To measure the offset of the inertial MEMS, the PCB channels were previously set, using the potentiometers, to have an offset negligible compared to the one of the MEMS.

Axis	card#4 offset(V)	card#5 offset(V)
X1	-0,0262	0,017
Y1	0,0002	-0,03
Z1	-0,0134	-0,0147
X2	-0,0257	-0,0014
Y2	-0,0127	-0,0195
Z2	-0,0123	-0,0085
X3	0,0077	-0,0449
Y3	-0,0285	-0,0005
Z3	-0,024	-0,0195

Figure 32: Offset measurement of each channel of both PCBs before connecting the inertial MEMS.

The PCB5 has been used for the self-test on the Z axis only and PCB4 for the axes X and Y. Calculating the difference that will be induced at the Full Scale is tedious because the Full Scale also depends on the sensitivity that can be very different according to the self-test or the ± 1g measurement. To be sure that this offset does not impact the final Full Scale measurement, the calculation has to be done for the measurements of the same magnitude as the last figure (i.e. a 0g measurement of tenths of mV). The difference was negligible every time.

7.2.2 Hysteresis

When measuring ± 1g or testing the self-test measurement, the initial output and the final output (after the ± 1g or the self-test) are different for the same input. It shows the hysteresis effect of the MEMS transducer. It can be noticed that the variability of this value depends on the MEMS. The hysteresis has been calculated for both self-test and ± 1g measurement methods.

7.2.3 self-test measurement

The self-test consists of changing the test voltage. There are 2 cycles: X/Y axes V_{test}=[0,16,32,64,32,16,0](PCB4) and Z axis: V_{test}=[0,5,10,15,10,5,0](PCB5). The self-test built in the Z axis is not the same as the ones of X/Y axes and consequently, the maximum test voltage is lower. Indeed, the MEMS must be able to survive a one-time 10000g event. FEM simulations have shown that a contact could happen between the proof mass and the electrode at $\tilde{6}$579g and that is the main reason why a specific stopper has been designed for X/Y axes. A parallel plate configuration has been chosen for the Z axis, where the actuation voltage modifies the gap distance. This last configuration lowers the voltage as the static field is the same and the electrode surface is larger.

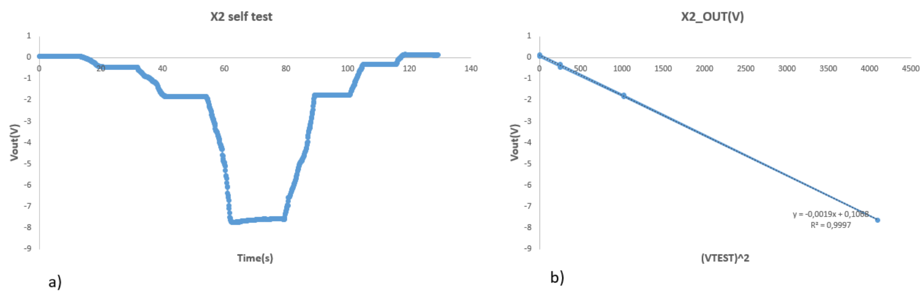

Figure 33: (a) self-test measurement. (b) Output voltage according to the square of the applied test voltage. It proves that they are proportional as in Figures 8 and 9.

There is an equation that links F.S.(g) measurements to the sensitivity(V/V/g):

$$Sensitivity = \frac{V_{out}}{V_{pol}.Gain.F.S.} \tag{10}$$

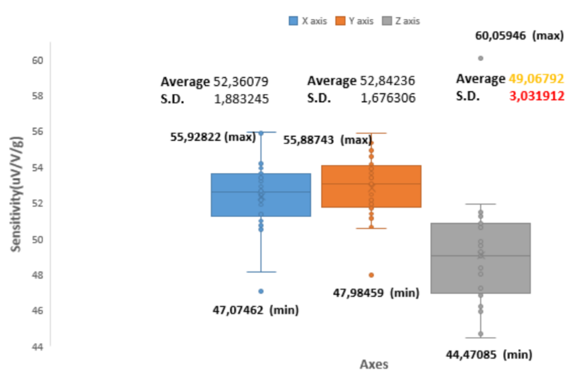

Figure 34: Histogram of the measured sensitivities using the self-test method for 30 samples/axis (There are 10 boards with 3 accelerometer/axis each).

The formula is used to calculate the sensitivity at maximum test voltage (15V or 64V according to the axis). The values can be compared to the ones obtained in figures 9 and 10 (roughly 70% of the F.S. or 700g). The self-test measurement has been done for 10 MEMS in order to determine the sensibility of each axis.

As the measured sensitivities seem coherent, the curves obtained in Figures 9 and 10 can be reproduced using this time experimental values.

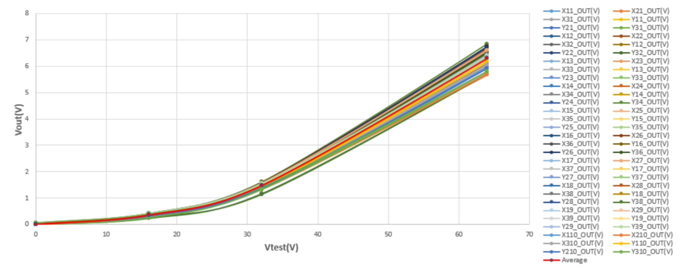

Figure 35: Self actuation voltage according to the applied test voltage for X and Y axes of the 10 MEMS.

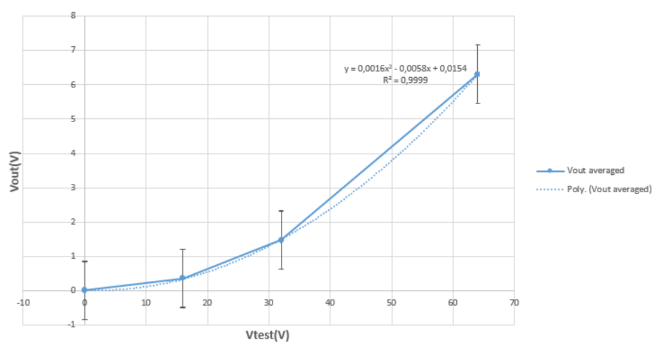

Figure 36: Average of all measured X/Y axis and a polynomial fitting of degree 2.

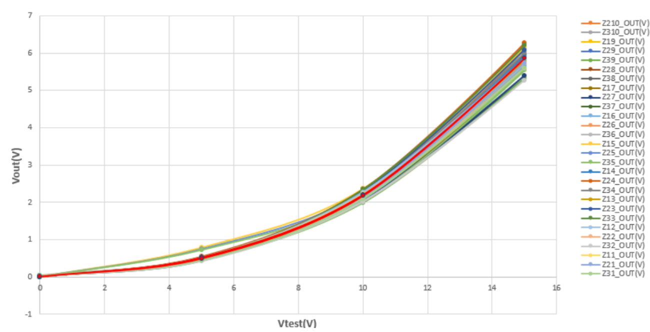

Figure 37: Self actuation voltage according to the applied test voltage of Z axis of the 10 MEMS.

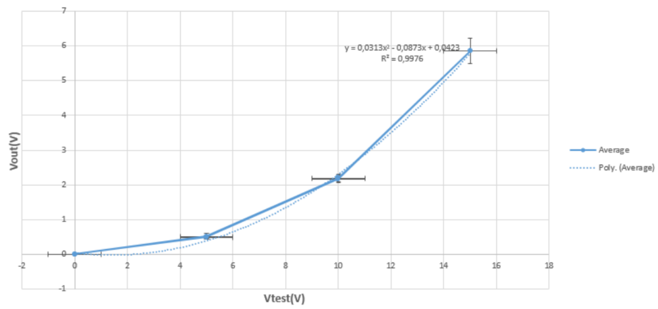

Figure 38: Average of all measured Z axis and a polynomial fitting of degree 2.

7.2.4 ± 1g F.S. measurement

The ± 1g test works well in most of the MEMS. A step is seen in the signal when the acceleration is modified.

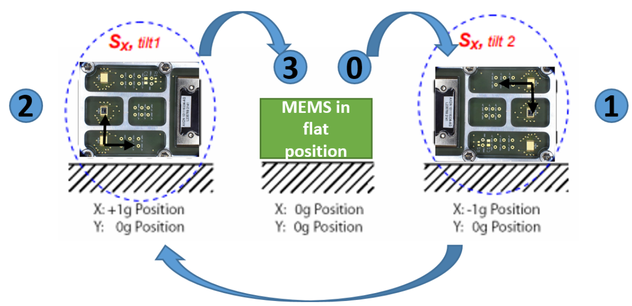

Figure 39: ± 1g measurement's procedure.

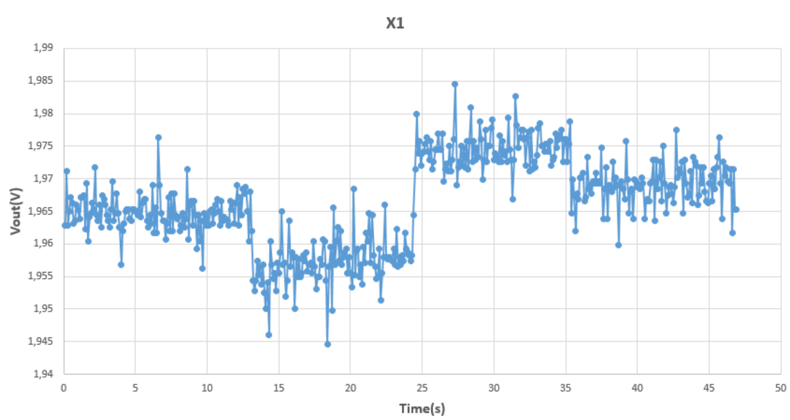

Figure 40: ± 1g measurement of X2 axis.

However, when the sensibility is computed, the standard deviation is much higher compared to the self-test method and to the requirements (sensitivity accuracy larger than 10%).

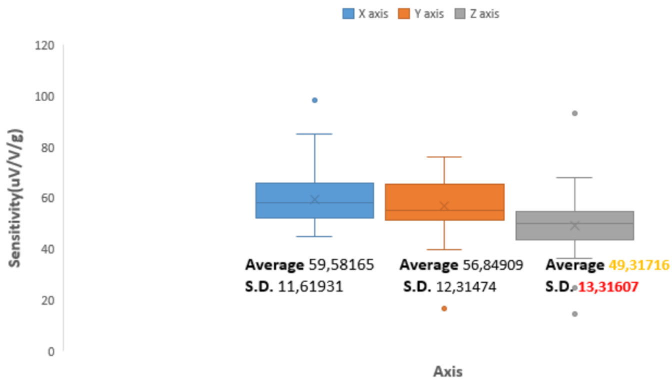

Figure 41: Histogram of the measured sensitivities using the ± 1g measurement method for 30 samples/axis (There are 10 boards with 3 accelerometer/axis each).

7.3 Noise characterization

The PCB's noise can be measured just by connecting the 2 differential inputs together and looking at the output voltage of the PCB. The RMS value found is around 1mV and the maximal allowed output is around 9.1V. Therefore, the SNR can be calculated.

$$SNR_{PCB} = 20.log(V_{out}/Vmin) = 79.1dB \tag{11}$$

This noise is added in parallel to the other existing noises in the MEMS. The overall noise can be calculated using Equation 3.

$$\frac{1}{SNR^2} = \frac{1}{SNR_{TH}^2} + \frac{1}{SNR_{FL}^2} + \frac{1}{SNR_{PCB}^2} \tag{12}$$

If an assumption is made supposing that the thermal noise of the MEMS can be neglected. $SNR_{FL}(dB)$=142.62 dB using the values from previous studies [2]. Therefore, the overall SNR is roughly 79dB. There is an error percentage of 1.25% with respect to the requirements (SNR > 80dB) which is acceptable because the output variation corresponds to the variation of the gain (i.e. figure called ***Gain of each channel of the 5 PCB and its standard deviation in %.***), both are of the same magnitude.

7.4 Shock study

7.4.1 Test objective and plan

The purpose of this test is a characterization of the MEMS using the PCB to record several axes at the same time. At the end, the match between the reference signal and the channel signals will be observed and the Full Scale will be compared with respect to the specifications in order to confirm the functionality. The level of shock is within 850-1100 g in association with single-axis reference accelerometers. Each axis (X, Y, and Z) is tested. Tests are repeated at ambient temperature (23-25 °C). Multiple devices are tested (two or three devices per board, per axis). Consequently, the test plan is varying test conditions versus axis/position and temperature mainly. Only the old MEMS were tested. Shock tests on the new MEMS should be carried out in the future.

The MEMS transducer is mounted on a board. Three MEMS transducers are mounted per board with a 1000g range.

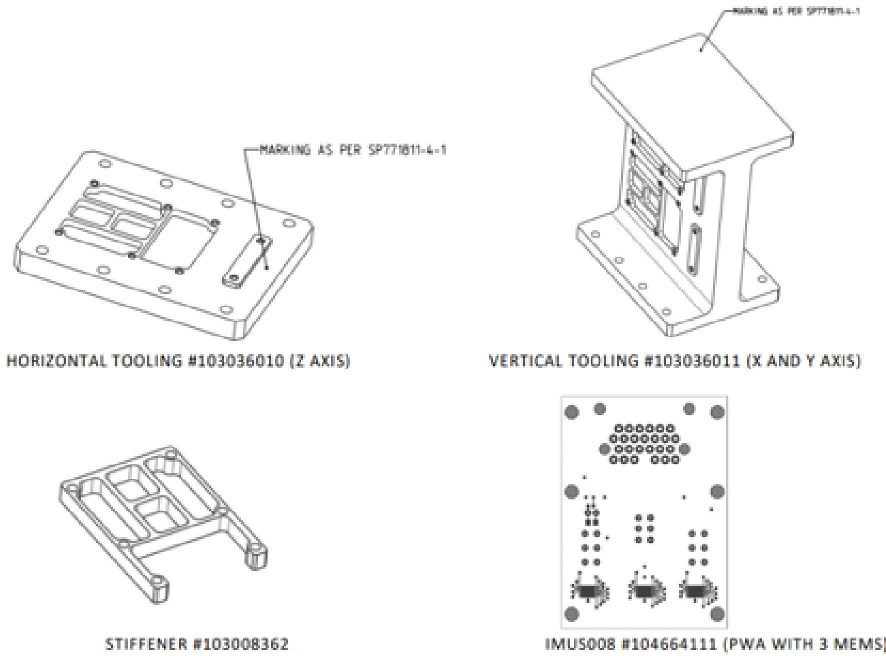

Figure 42: Test setup tooling.

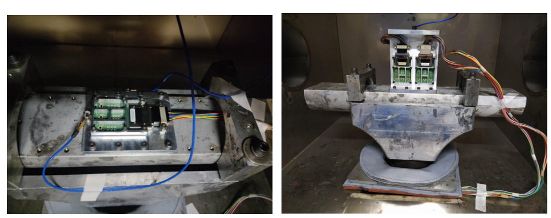

(a) (b)

Figure 43: (a) MEMS transducer wiring diagram, Z position. (b) MEMS transducer wiring diagram, Y position.

Analog MEMS Wheatstone bridge is supplied (Vpol) from a power supply (Keithley 2450) with a current source imposed (3mA to 4mA) and its output channels are amplified (amplifier powered by +/- 15V). Signals are captured by a multi-channel DAQ from Keysight (U2355A). Acquisition is using INA103 amplifiers as analog front-end, the theoretical gain is 452,1 (each gain is characterized for accurate scale factor computations). Therefore, the acquisition chain uses the following settings:

- Vpol: 3mA to 4mA current source (typical range is 0.3V to 0.5V depending on test board impedance).
- Gain: 452.1
- Sampling: 25 kS/s.
- Resolution: 16 bits.
- Range: +/-10V.

7.4.2 Results

At the end, the role of the PCB is mainly to allow the recording of several accelerometers. As a result, it is also important to see its performance in real conditions using a vibrator test bench. The experiments show that it works very well but a difference between the reference sensor measurement and the one made by the MEMS has been seen.

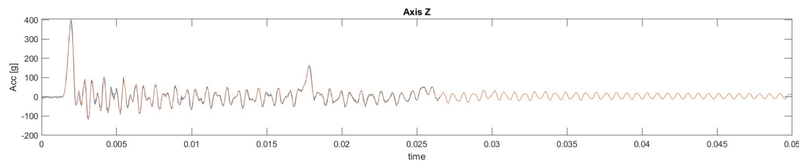

(a) Input acceleration peak around 400g

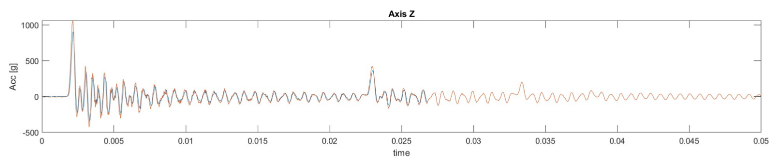

(b) Input acceleration peak around 1050g

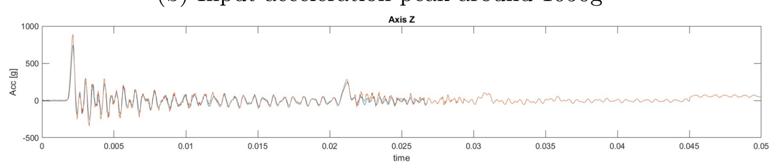

(c) Input acceleration peak around 850g

Figure 44: Shock waves of the Z1-axis of the MEMS number 10 for three input accelerations. In orange is the reference sensor and in blue is the inertial MEMS.

To determine the origin of this variation, a sequence of measurements was organized. Hundreds of shocks in different axis positions were performed. The results show that, in general, when the accelerator is functional, the variation is linear for an acceleration lower than 1000g (an input acceleration of 1000g, will reach the Full Scale value of the DAQ). After 1000g, in most of the MEMS a saturation is seen. This trend has been seen using MEMS with a good sensitivity (50uV/V/g). Consequently, the sensitivity would shift the saturation value of the MEMS to lower or higher accelerations if the sensitivity is higher or lower (respectively).

In the figure called ***Shock waves of the Z1-axis of the MEMS number 10 for three input accelerations. In orange is the reference sensor and in blue is the inertial MEMS.***. Both signals fit very well, there is a fidelity not only reproducing the main shock but during all time of acquisition. There is a gap between the peaks of the reference sensor and the measured axis but it is not a problem. Plotting the acceleration output of the measured axis according to the acceleration of the reference sensor, linearity is seen between both outputs (it is shown in a figure called ***Acceleration accuracy on the vibrator test bench. Sequence A MEMS board10. Most of the functional MEMS have a linear behavior below 1000g. Above 1000g saturation in some MEMS can be noticed because of the offset.***).

Sequence	Position / Axis	Temperature	MEMS Board	Acquisition Board	Amplitude	Shocks
A	Z	20-25 °C	10	1	1000g	100
B	Z/X 45°	20-25 °C	10	1	1000g	100
C	Z	20-25 °C	9	1	1000g	100
D	Z/X 45°	20-25 °C	9	1	1000g	100
E	X	20-25 °C	9	1	1000g	100
F	X	20-25 °C	10	1	1000g	100
G	Y	20-25 °C	9	1	1000g	100
H	Y	20-25 °C	10	1	1000g	100
I	Y	20-25 °C	10	2	1000g	100
J	Y	20-25 °C	10	3	1000g	100

Figure 45: Shock sequences. If the cross-axis effect were visible the sequences B and D would amplify it.

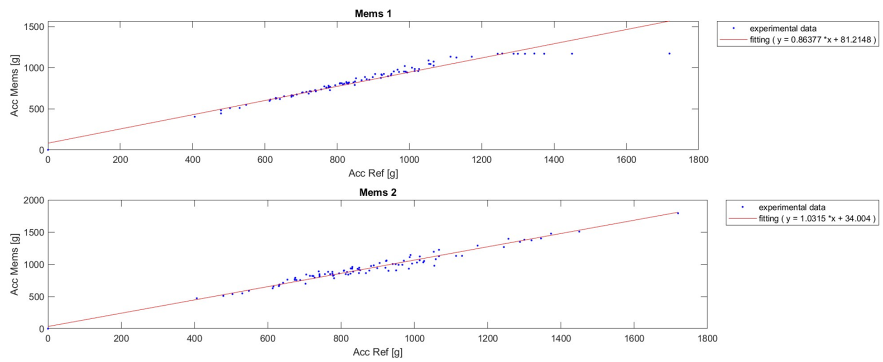

Figure 46: Acceleration accuracy on the vibrator test bench. Sequence A MEMS board10. Most of the functional MEMS have a linear behavior below 1000g. Above 1000g saturation in some MEMS can be noticed because of the offset.

8 Discussion

To resume, the final goal of the ESIP project is to achieve a longer lifetime of downhole tools used in the drilling of oil wells. In order to do that, a sensor able to measure several parameters, such as the shock levels of the tool at a given depth (using an accelerator/ inertial sensor), the pressure, the temperature, or even the humidity is needed and the ESIP sensor has all these features included.

The first aim of the internship was to conceive a functional PCB to record data of one inertial MEMS (only the three accelerometers) and the reference sensor. In the section 7, shock experiments in real conditions were carried out and showed that the PCB works well. The offset is not a problem anymore and the flat bandwidth allows to have a stable gain for the working frequencies of the sensor. Although, there are several modifications that could improve the performance and to better fit with the requirements.

- The gain accuracy of 1% can be easily achieved by replacing the passive components of the pass-band filter with more accurate ones (below 1%). It could take more time to deliver because those components are more difficult to find.
- The connectors can be more spaced, and the holes displaced a bit more to the center of the PCB.
- Change some connections to avoid making straps.
- Make two independent self-test channels (one for the X/Y axes and another for the Z axis).
- Put decoupling capacitors to all the power signals. The instrumental amplifiers have a slew rate of 15V/us and the operational amplifiers have a slew rate at a unitary gain of 0.5V/us. Consequently, in the worst-case scenario, the overall capacity is 75nF. If a bit of margin is kept, capacitors of 100nF will be enough.

- Utilization of slide switches to perform AC and DC studies on the same PCB.

Concerning shock recordings, the whole system works very well at the aimed range (up to 1000g) and the values are repeatedly coherent. The cross axis effect is negligible (see Appendix).

The DC study has several information about the setup and the experiments that will be carried out in the future. First, if the figures ***Histogram of the measured sensitivities using the self-test method for 30 samples/axis (There are 10 boards with 3 accelerometer/axis each).*** and ± ***2g Histogram of the measured sensitivities using the self-test method for 30 samples/axis (There are 10 boards with 3 accelerometer/axis each).*** are compared, three main information can be extracted: The self-test method is more accurate than the ± 2g measurement method, the X and Y axes seem to be identical in terms of sensitivity (to be confirmed by shock tests using the new MEMS) and the sensitivity of the Z axis seems to be lower, as the self-test design is different from the X and Y axes.

The figure called ***Average of all measured X/Y axis and a polynomial fitting of degree 2.*** allows us to reproduce the simulated curve in Figure 9. As the correlation coefficient shows, the fitting curve matches very well on this axis. A relative dispersion of 5.4% is found.

The figure called ***Average of all measured Z axis and a polynomial fitting of degree 2.*** allows us to reproduce the simulated curve in Figure 10. The correlation coefficient is a bit lower this time but it is still good. A lower relative dispersion of 4.6% is found.

Both relative dispersions are below 10% and that is good news. The self-test method could be used to avoid calibrating the MEMS individually and reduce its cost price. The accuracy can still be improved, for instance using a more sophisticated setup using shorter and shielded cables. Besides, when the MEMS is produced at a large scale, the functions of the PCB would be done on an ASIC which has a lower noise. If the possible final MEMS product is compared with other existing inertial MEMS using the same technology [14] (TE 500g 832M1. It costs around 150$), the ESIP MEMS would record several axes, it would also record the pressure and the humidity, it would have a better sensitivity and it could work at high temperature. The price would be around 250$. Consequently, there is an economic and technical interest in this project.

Shock tests of the new generation of inertial MEMS (with better sensitivity and better repeatability) would confirm the sensitivity values and the partial conclusions obtained during the DC study. A summary of the measurements will be available in the Appendix section.

9 Conclusion

During the internship, the main challenge was to make work all the parts of the project together, but in the end, it was operational and the project could continue improving. Therefore, a sensibility value of both axes, with an accuracy of 5% or lower, could be possible. The next steps will be: to record as much data as possible during shock simulations using the new generation of MEMS, to carry out 4g measurement tests to get more accurate values than using ± 1g F.S. measurement, to simulate the MEMS on COMSOL verify its operation, and also that there is no external constraint that could bias the measurement. Other parts of the MEMS, such as the pressure sensor, the temperature sensor, and the humidity sensor should be characterized before designing it at high volume. The data obtained can be also used to verify if there are systematic errors during the microfabrication that could damage specific functions of a MEMS in a certain area of the wafer.

10 Personal advantages

Choosing the SLB as a company gives you visibility and perspectives worldwide. The research done is at a very high level with ambitious plans and long-term projects in order to maintain its place as the first equipment provider in the oil and gas industry. It is a company in which you can develop your skills and you can reach very high positions if you are determined and mobile all around the world. The working conditions are excellent, but constant improvement is required to not be left behind in this very competitive field.

11 Project outline

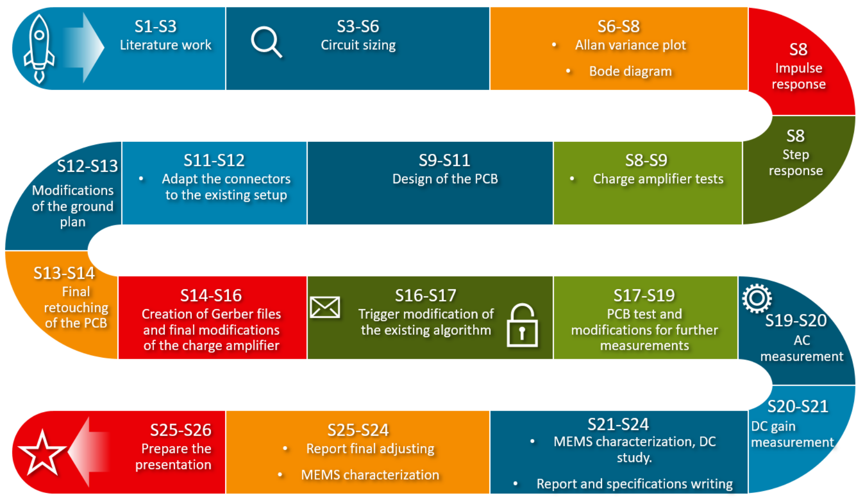

Figure 47: Project outline.

This is the current project outline. Of course, it differs from the project outline expected initially. Indeed, the circuit sizing part took more time than expected because another circuit with an automatic restoration offset had been studied before choosing the current option present in the MEMF001 using potentiometers. The PCB design was also longer because there were unexpected issues with the charge amplifier part and additional precaution was taken in choosing the components to avoid a serious malfunction that could stop the project or deviate it from its initial goal. Everything was linked, there were different interfaces and in the end, the difficulty resided in making work everything together. During the end of the internship, overtime was necessary because the new MEMS arrived later than expected and the DC measurements were made during the last week. Despite all these problems, the main goal of the internship, which was the characterization of the inertial MEMS, has been reached on time.

12 Bibliography

[1] Donald Knuth. Schlumberger - Who we are. https://www.slb.com/who-we-are.(visited on August 2023).

[2] ESIP - MEMS Design - L2.3. CEA Leti and Schlumberger (SLB). Project code: S35270/3. N/ Ref.: LETI/DSYS/SSCE/LAIC/2021-0287/JW.(visited on August 2023).

[3]Y. Sun, Strain Effect in Semiconductors - Theory and Device Applications. Springer, 2010. http://www.springer.com/la/book/9781441905512.(visited on August 2023).

[4] S. Dellea, F. Giacci, A. F. Longoni, G. Langfelder, P. Rey, et P. Robert, « Analysis of gyrocompassing through miniaturized MEMS based on piezoresistive sensing », in 2016 IEEE International Symposium on Inertial Sensors and Systems, févr. 2016, p. 25-28. DOI: 10.1109/ISISS.2016.7435536.(visited on August 2023).

[5] J. C. Doll, S.-J. Park, et B. L. Pruitt, « Design optimization of piezoresistive cantilevers for force sensing in air and water », J. Appl. Phys., vol. 106, no 6, p. 064310, sept. 2009, DOI: 10.1063/1.3224965.(visited on August 2023).

[6] Keysight U2300A Series USB Multifunction Data Acquisition Devices.(visited on August 2023).

[7] P.Rey D.Dezest. ESIP - MEMS Design Report- L2.3. 1. 2021, pp. 15–120.(visited on August 2023).

[8] INA103KP Low Noise, Low Distortion Instrumentation Amplifier datasheet. Burr-Brown Corporation.https://urlz.fr/nePU.(visited on August 2023).

[9] Introduction to Allan Variance—Non-overlapping and overlapping Allan Variance - technical articles. https://urlz.fr/nePI. (visited on August 2023).

[10] Charge Amplifier Circuit.Texas Instruments.(visited on August 2023).

[11] LM348n Precision Reference datasheet. Texas Instruments Incorporated.https://www.ti.com/product/LM348?utm_source=google&utm_medium=cpc&utm_campaign=asc-null-null-GPN_EN-cpc-pf-google-eu&utm_content=LM348&ds_k=LM348+Datasheet&DCM=yes&gclid=EAIaIQobChMI_5irwoL_gAMVzd_tCh00OAz2EAAYAiAAEgJvzfD_BwE&gclsrc=aw.ds.(visited on August 2023).

[12] ESIP PROJECT Deliverable L2.13- Report on wafer-level tests. Project code: ESIP. N/Ref. : DRT-LETI-DCOS-SITE-LICA-22-09-00267.(visited on August 2023).

[13] Shock testing & analysis. enDAQ. https://endaq.com/pages/shock-testing-analysis. (visited on August 2023).

[14] Model 832 / 832m1 accelerometers - TE connectivity | DigiKey. https://www.digikey.fr/fr/product-highlight/t/te-connectivity-measurement-specialties/model-832-832m1-accelerometers.(visited on August 2023).

13 Abstract in English

Sensors are used to detect changes on the ground during drilling and the aim of the project is to further develop the ESIP project (Enviromental System In Package). This project focuses on the design of an accelerometer, a pressure sensor, a temperature sensor, and a humidity sensor. Last year, a PCB (printed circuit board) was made to transform the acceleration (shock) into an electric signal. The goal of the internship is to resume the project of creating an electronic card that will filter and amplify (to the Full Scale allowed at the output of the whole system) the incoming signal of each accelerometer of the MEMS (9 axes in total), the electronic card also has to be able to reduce the offset that could induce saturation. The PCB will be first characterized alone, to be sure of its functionality and its performance. Then, it will be used to characterize all the inertial MEMS and obtain the sensibility, the hysteresis, etc. Shock experiments and characterizations will be made, in real conditions, to verify MEMS performance and compare it to the expected requirements, in terms of accuracy and linearity.

14 Résumé

L'objectif du projet ESIP (Enviromental System In Package) est de déployer une nouvelle génération de capteurs sur le terrain qui sont plus précis, plus compacts et plus résistants. Dans le cadre du stage, le but principal est de concevoir une PCB qui reçoit les signaux de chaque accéléromètre(9 axes en tout) en filtrant et en amplifiant le signaux et diminuant l'offset de chaque axe afin d'utiliser la plus grande plage de valeurs en sortie. Ensuite, des caractérisations seront menés, d'abord pour valider la PCB, puis sur le MEMS afin de connaître précisement les paramètres de chaque axe tels que la sensibilité, l'hystéresis, etc. Des expériences de shock seront aussi effectués en conditions réelles pour vérifier et comparer avec le cahier des charges specialement en termes de précision and linéarité.

15 Abstract in Italian

sensori vengono utilizzati per rilevare i cambiamenti sul terreno durante la perforazione e l'obiettivo del progetto è quello di sviluppare ulteriormente il progetto ESIP (Enviromental System In Package). Questo progetto si concentra sulla progettazione di un accelerometro, un sensore di pressione, un sensore di temperatura e un sensore di umidità. L'anno scorso è stato realizzato un PCB (circuito stampato) per trasformare l'accelerazione (shock) in un segnale elettrico. L'obiettivo del tirocinio è quello di riprendere il progetto realizzando una scheda elettronica che filtrerà ed amplificherà (fino al Fondo Scala consentito all'uscita dell'intero sistema) il segnale in ingresso di ciascun accelerometro del MEMS (9 assi in totale), il la scheda elettronica deve inoltre essere in grado di ridurre l'offset che potrebbe indurre saturazione. Il PCB verrà prima caratterizzato da solo, per essere sicuri della sua funzionalità e delle sue prestazioni. Quindi, verrà utilizzato per caratterizzare tutti i MEMS inerziali e ottenere la sensibilità, l'isteresi, ecc. Verranno effettuati esperimenti e caratterizzazioni di shock, in condizioni reali, per verificare le prestazioni dei MEMS e confrontarle con i requisiti previsti, in termini di accuratezza e linearità.

16 Appendix

16.1 Acceleration accuracy on the vibrator test bench

16.1.1 Sequence A

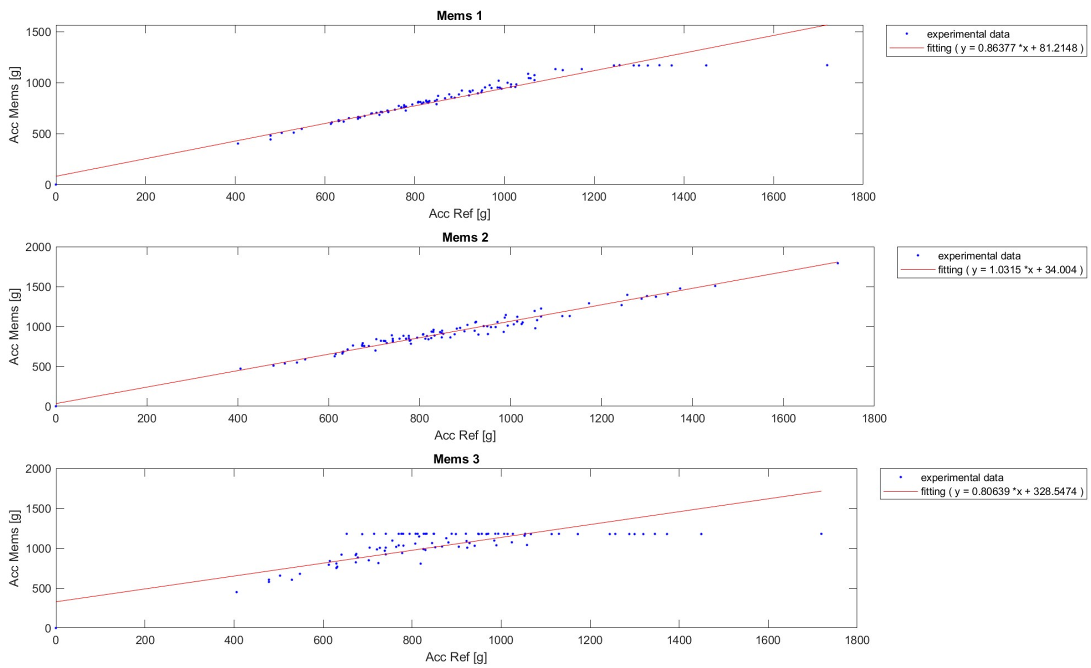

Figure 48: Acceleration accuracy on the vibrator test bench. Sequence A

16.1.2 Sequence B

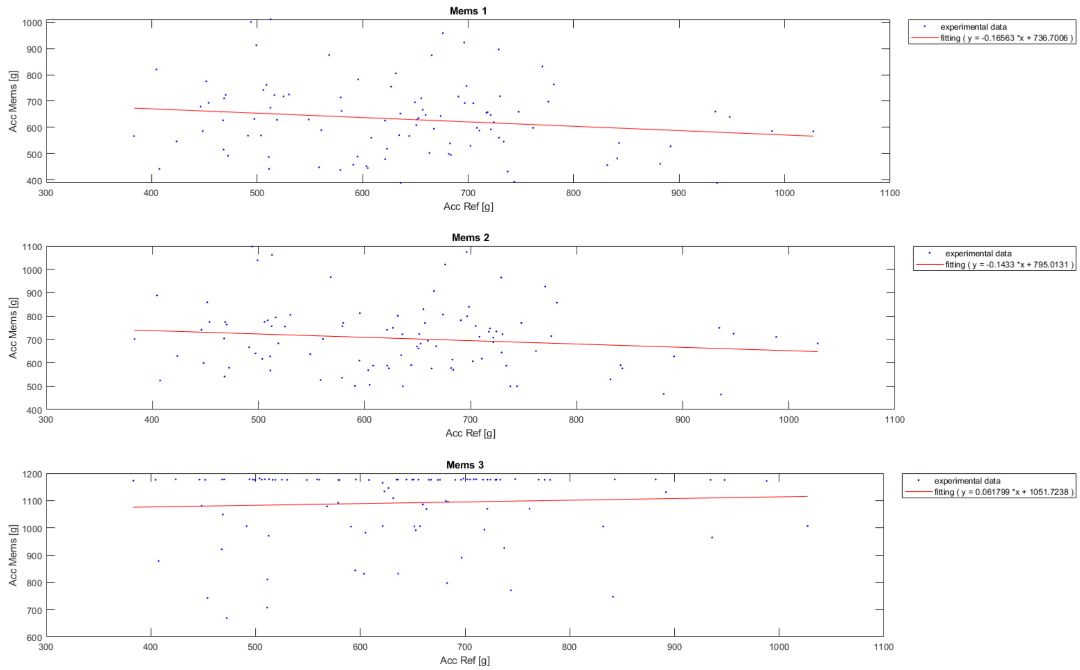

Figure 49: Acceleration accuracy on the vibrator test bench. Sequence B

16.1.3 Sequence C

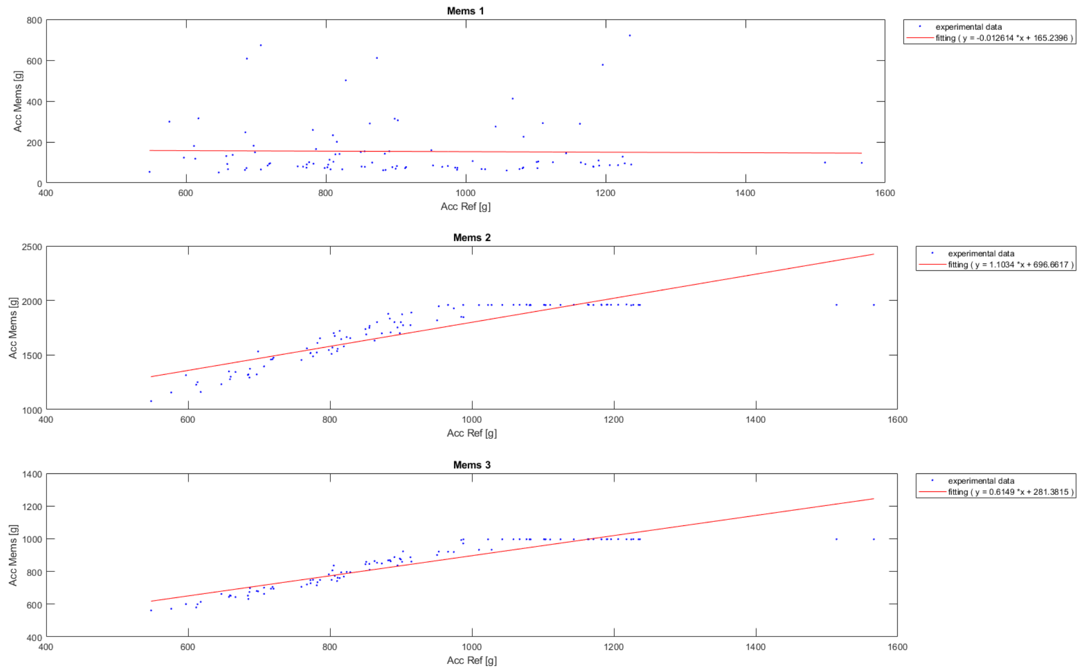

Figure 50: Acceleration accuracy on the vibrator test bench. Sequence C

16.1.4 Sequence D

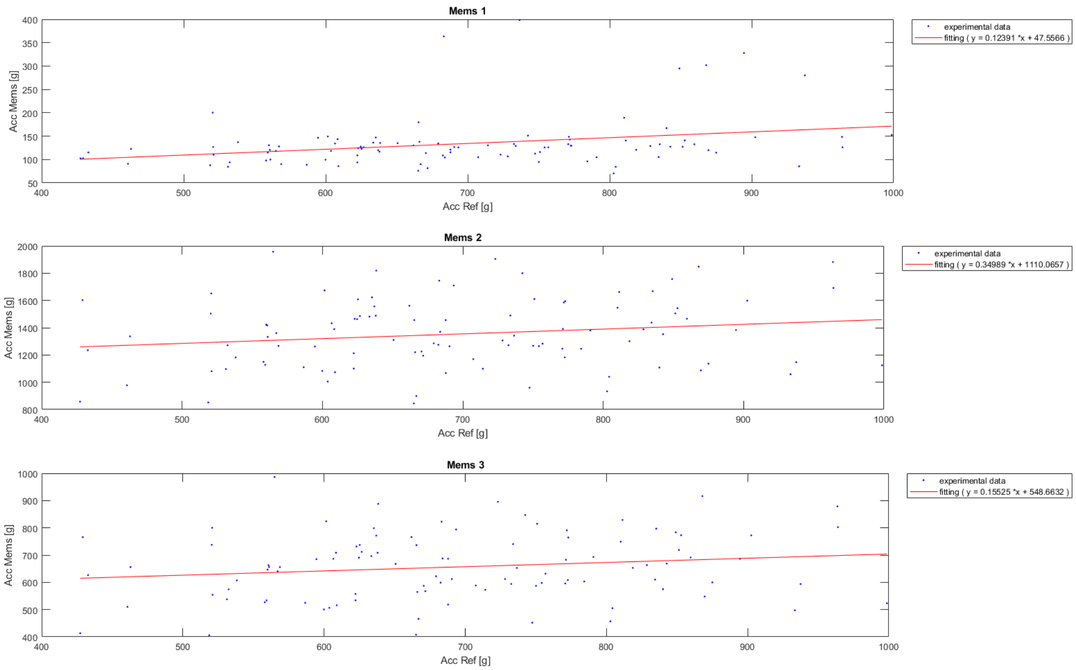

Figure 51: Acceleration accuracy on the vibrator test bench. Sequence D

16.1.5 Sequence E

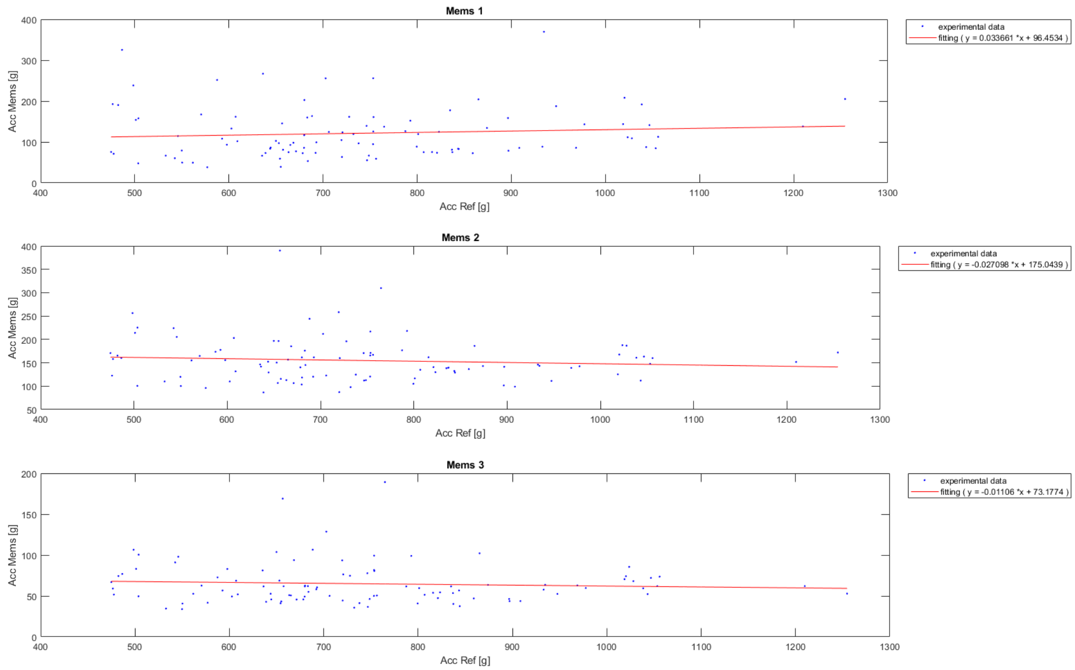

Figure 52: Acceleration accuracy on the vibrator test bench. Sequence E

16.1.6 Sequence F

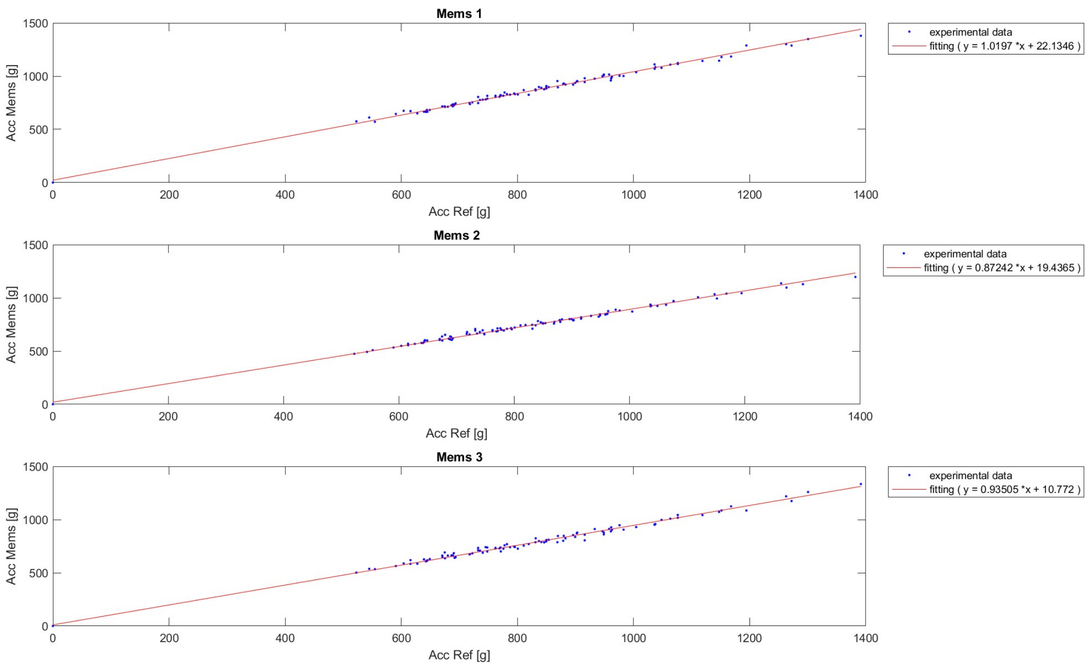

Figure 53: Acceleration accuracy on the vibrator test bench. Sequence F

16.1.7 Sequence G

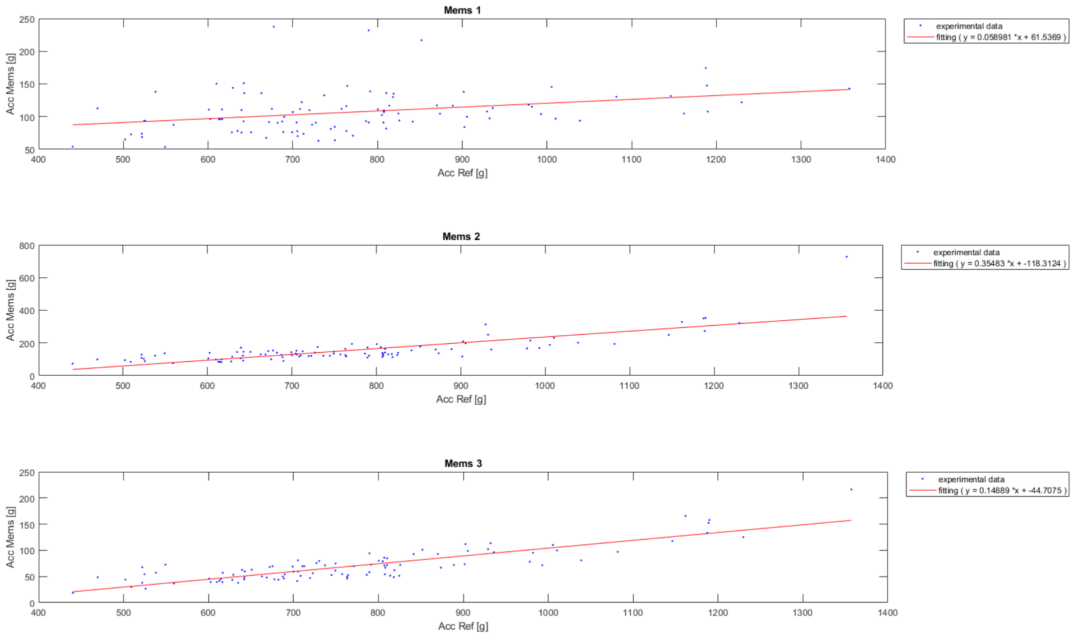

Figure 54: Acceleration accuracy on the vibrator test bench. Sequence G

16.1.8 Sequence H

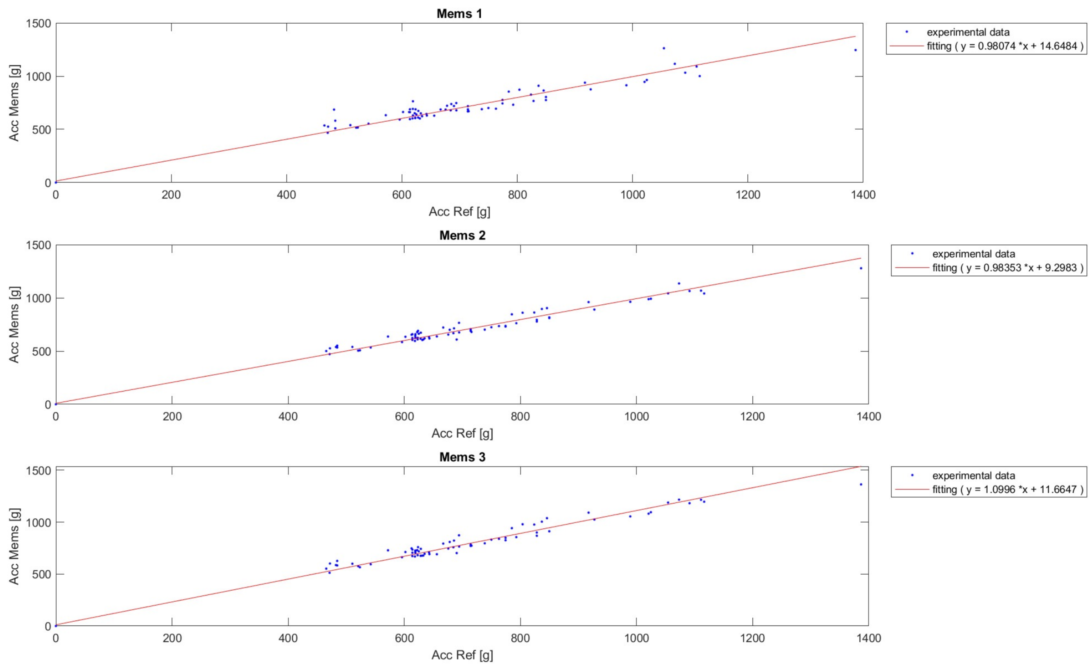

Figure 55: Acceleration accuracy on the vibrator test bench. Sequence H

16.1.9 Sequence I

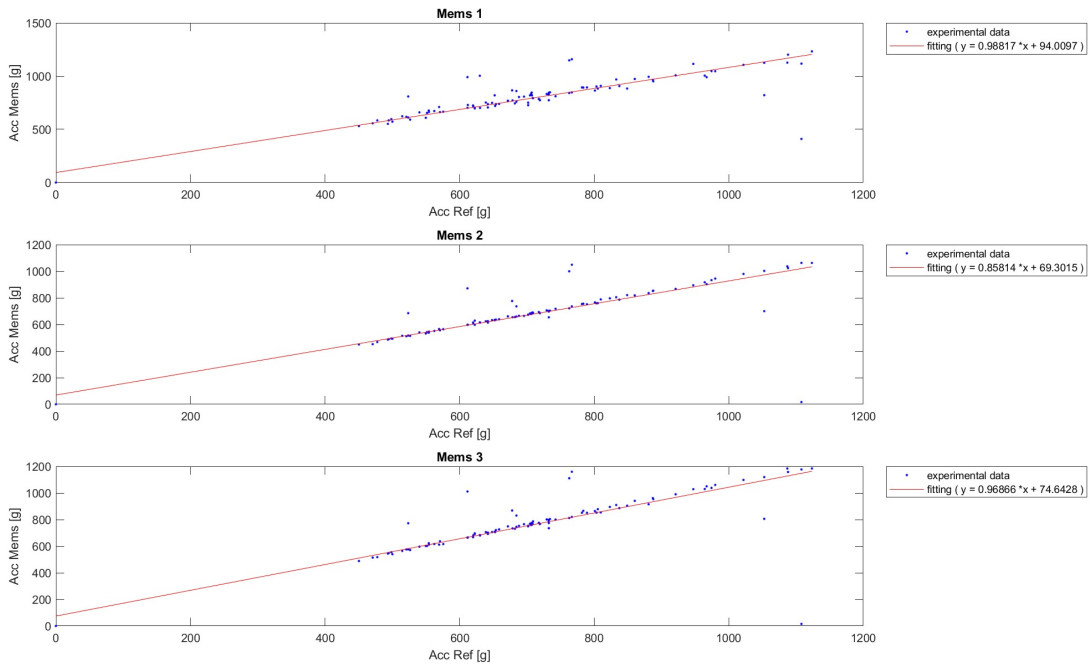

Figure 56: Acceleration accuracy on the vibrator test bench. Sequence I

16.1.10 Sequence J

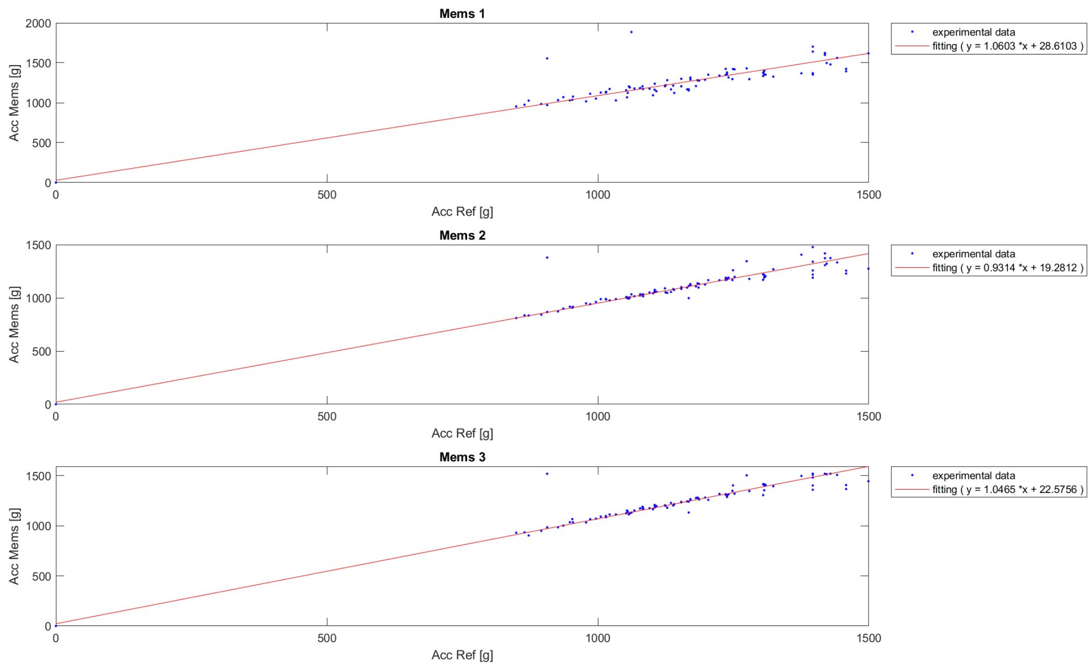

Figure 57: Acceleration accuracy on the vibrator test bench. Sequence J

16.2 Sensitivity calculated using ± 1g F.S. and self-test methods

A color code is used. Red stands for the bad values (no coherent. The offset is higher than 50% or the sensitivity above 65 uV/V/g or below 30 uV/V/g), yellow is used for the acceptable ones (Offset between 30% and 50% and sensitivity between 30 and 40 or between 60 uV/V/g and 65 uV/V/g) and green is used for the good ones (offset below 30% and sensitivity between 40 uV/V/g and 60 uV/V/g).

%F.S.(g) stands for the percentage of Full Scale acceleration with respect to the maximal acceleration allowed (in theory 1000g).

16.2.1 Sensitivity calculated using ± 1g F.S. method. Old MEMS

Chip	IMUS008 Test board	Axis	Offset (% F.S.)	+/-1g Sensitivity (uV/V/g)	Offset test Vpol (V)	Vout at +1g (V)	Vout at -1g (V)	Hysteresis(V)
G5B2	3	X1						
	3	Y1						
	3	Z1						
B4B2	3	X2						
	3	Y2						
	3	Z2						
D3B6	3	X3	28,40763359	56,71981611	0,394059	2,833709717	2,85369873	0,007629395
	3	Y3						
	3	Z3	18,40340909	76,2640832	0,394059	-2,457733154		0,009460449
C4B8	4	X1						
	4	Y1						
	4	Z1						
B8B8	4	X2						
	4	Y2						
	4	Z2						
C8B5	4	X3						
	4	Y3						
	4	Z3						
A3B8	5	X1						
	5	Y1						
	5	Z1	8,937096774	63,43186253	0,333	0,836029053		
F4B7	5	X2	11,83909774	68,20664274	0,333	-1,204376221	-1,184082031	0,003662109
	5	Y2						
	5	Z2						
C8B6	5	X3	25,4752	63,76697655	0,33292	2,440490723	2,421417236	0,001831055
	5	Y3						
	5	Z3	23,04912281	58,45602159	0,333	-1,996002197		0,005340576
C4B3	6	X1	63,98640777	58,23787164	0,30277	5,02532959	5,041046143	0,007476807
	6	Y1						
	6	Z1	50,75079365	70,89044723	0,30277	4,888305664		-0,001220703
A6B2	6	X2	10,11588785	60,35179654	0,30277	0,830841064	-0,81451416	0,006713867
	6	Y2						
	6	Z2	30,9775	45,1533269		1,896820068		0,000305176
C4B4	6	X3	6,630952381	47,33596277	0,30277	-0,42755127	-0,414733887	0,002593994
	6	Y3						
	6	Z3						

Figure 58: Sensitivity calculated using ± 1g F.S. method. First part. Old MEMS

Chip2	IMUS00B Test board3	Axis4	Offset (% F.S.)5	+/-1g Sensitivity (uV/V/g)6	Offset test Vpol (V)7	Vout at +1g (V)8	Vout at -1g (V)9	Hysteresis (V)10
C8B8	7	X1	17,4656	50,3006064	0,42542	1,654663086	1,673736572	0,001525879
	7	Y1						
	7	Z1						
B8B7	7	X2						
	7	Y2						
	7	Z2	98,61666667	48,20320901	0,42542	9,037780762		0
C3B5	7	X3	26,25098039	20,45394304	0,42542	1,011657715	1,019439697	0,015869141
	7	Y3						
	7	Z3						
E2E4	8	X1	28,71318681	76,48837597	0,40734	3,975524902	4,003295898	0,007781982
	8	Y1	2,823255814	35,96428281	0,40734	0,191802979		0,001831055
	8	Z1						
B5B5	8	X2	19,21044776	56,1780946	0,40734	1,955108643	1,97555542	0,002593994
	8	Y2						
	8	Z2	12,25087719	47,82559709	0,40734	-1,05682373		0,003662109
G5B6	8	X3		59,89681753	0,40734			
	8	Y3						
	8	Z3	3,410465116	72,10079025	0,40734	-0,434417725		0,007171631
B4B8	9	X1						
	9	Y1						
	9	Z1						
D5B7	9	X2	3,434482759	30,4533031	0,48787	-0,220836914	-0,207061768	0,023193359
	9	Y2						
	9	Z2	96,22911389	19,63855625	0,48816	-4,121551514	-4,113006592	-0,016021729
F2B5	9	X3						
	9	Y3						
	9	Z3	43,47	48,99960276			-4,621734619	0,016021729
G7B3	10	X1	12,67336927	51,43079411	0,466	1,340942383	1,362304688	0,001025042
	10	Y1	36,85866667	54,76182252	0,466	4,206542969	4,229431152	-0,001373291
	10	Z1	13,6137931	84,80707413		2,392730713	2,428131104	-0,009002686
C6B8	10	X2	29,92265193	66,0069439	0,46548	4,120178223	4,147796631	0,00579834
	10	Y2						
	10	Z2						
E4B8	10	X3	16,10348259	73,33659308	0,46548	2,459564209	2,490234375	-0,020446777
	10	Y3						
	10	Z3						

Figure 59: Sensitivity calculated using ± 1g F.S. method. Second part. Old MEMS

16.2.2 Sensitivity calculated using self-test method. Old MEMS

Chip	IMU5008 Test boa	Axis	Offset (% F.S.)	Self test Sensitivity (uV/V/g)	self test Vpol (V	Self test Vout @ 0V (V)	Self test Vout @ 64V (V)	Self test Hy
G5B2	3	X1						
	3	Y1						
	3	Z1						
B4B2	3	X2						
	3	Y2	70,303665	-16,46241884	0,39409	0,008830098	-2,048950195	0
	3	Z2						
D3B6	3	X3	39,31435	-52,58123666	0,39409	2,84576416	-3,659667969	-0,010681152
	3	Y3						
	3	Z3						
C4B8	4	X1						
	4	Y1	62,723124	-51,98264279	0,4045	0,640869141	-5,93170166	-0,047302246
	4	Z1						
B8B8	4	X2	70,182052	-78,37497505	0,4045	0,025939941	-10	0
	4	Y2	78,173769	-52,02457281	0,4045	-0,771789551	-7,390136719	0,000915527
	4	Z2						
C8B5	4	X3	69,855901	-57,10850888	0,4045	0,015563965	-7,249145508	0,000610352
	4	Y3	85,349617	-47,82919529	0,4045	-1,349182129	-7,434082031	-0,012207031
	4	Z3						
A3B8	5	X1						
	5	Y1	88,612739	-52,15617398	0,33292	-1,461486816	-6,920166016	-0,00793457
	5	Z1	69,358736	-14,76316428	0,333	0,873718262	1,526794434	-0,839231827
F4B7	5	X2	85,465484	-51,57704756	0,33292	-1,195068359	6,59576416	-0,001525879
	5	Y2						
	5	Z2						
C8B6	5	X3	41,292135	-57,59579075	0,33292	2,481689453	3,55682373	0,008850098
	5	Y3	66,816375	-56,34430267	0,33292	0,269165039	-5,642700195	0,000305176
	5	Z3						
C4B3	6	X1	4,6978818	-56,46451784	0,30804	5,107421875	-0,367431641	0
	6	Y1	70	-59,64458855	0,30804	-5,784301758	-0,314941406	-0,314941406
	6	Z1	69,091661	-104,9044556	0,30277	4,956054688	9,999694824	4,914193741
A6B2	6	X2	70	-63,07678419	0,30804	-0,83770752	-6,112976074	-0,83770752
	6	Y2	70	-58,30329415	0,30804	-0,498657227	-5,647583008	-0,498657227
	6	Z2	69,860004	-104,0846807	0,30277	1,921081543	-10	2,072466543
C4B4	6	X3	70	-56,97062942	0,30804	-0,377197266	-5,518493652	-0,377197266
	6	Y3	70	-71,09936737	0,30804	-1,556396484	-6,902160645	-1,556396484
	6	Z3						

Figure 60: Sensitivity calculated using self-test method. First part. Old MEMS

Chip2	IMUS008 Test board	Axis4	Offset (% F.S.)5	Self test Sensitivity (uV/V/g) 6	selftest Vpol (V	Self test Vout @ 0V (V)	Self test Vout @ 64V (V	Self tes
C8B8	7	X1	52,66543	50,3176	0,426	1,670837	-5,07629	0
	7	Y1						
	7	Z1						
B8B7	7	X2						
	7	Y2	94,539	54,1853	0,426	-2,49634	-9,80316	0,048218
	7	Z2						
C3B5	7	X3	41,99841	-20,0749	0,426	1,074524	-1,61346	-0,00122
	7	Y3	70,17132	-74,3048	0,426	-0,0238	-10	0,00061
	7	Z3						
E2E4	8	X1	27,90363	58,0688	0,36381	3,998108	-2,65076	-0,00092
	8	Y1	76,7153	60,2682	0,36381	-0,66742	-7,56531	-0,00519
	8	Z1	78,46009	-78,2174	0,40734	6,612549	9,999695	6,601771
B5B5	8	X2	41,98519	42,8438	0,36381	1,96167	-2,94128	-0,00092
	8	Y2	80,84741	49,4217	0,36381	-0,86151	-6,53015	0,014648
	8	Z2	78,08294	57,1678	0,40734	-1,06903	7,250366	-1,04186
G5B6	8	X3	-25,5506	51,2304	0,36381	7,984924	2,139282	-0,01526
	8	Y3						
	8	Z3	78,25461	56,0976	0,40734	4,586182	7,135925	4,597208
B4B8	9	X1	91,00056	50,0613		-0,01831	-10	2,289429
	9	Y1						
	9	Z1						
D5B7	9	X2	68,76744	50,5569		0,058899	-7,62787	-0,07782
	9	Y2	82,95458	51,6483		-1,53503	-9,39575	-0,06775
	9	Z2	39,74056	62,7239		-4,13437	5,432587	0,002136
F2B5	9	X3						
	9	Y3						
	9	Z3						
G7B3	10	X1	56,94336	49,4574	0,46548	1,351013	-5,89478	-0,00061
	10	Y1						
	10	Z1						
C6B8	10	X2	34,6338	55,9668	0,46548	4,146423	-4,05518	0,005493
	10	Y2	66,46951	51,2178	0,46548	0,378418	-7,11884	0,000305
	10	Z2						
E4B8	10	X3	46,89596	51,3429	0,46548	2,47406	-5,03479	-0,00641
	10	Y3						
	10	Z3						

Figure 61: Sensitivity calculated using self-test method. Second part. Old MEMS

16.2.3 Sensitivity calculated using ± 1g F.S. and self-test methods. New MEMS

Chip	Test board	Axis	AVG Bridge	Bridge (Ohm)	Offset (% F.S.)	Sensitivity Hysteresis(V)	+/-1g Sensitivity (uV/V/g)	Self test sensitivity (µV/V/g)	Sensitivity die(uV/V/g)	Offset die % FS	% F.S. self test @64V	Delta Sensitivity (µV/V/g)	Hysteresis Self test @0V (V)	Comments
B3B5	1	X1	682,83	677,82	11	-0,00536152	61,92895202	53,20123665	57,12	10,58%	10,95680807	4	-0,033785419	
	1	Y1	682,83	688,72	0	-0,001166849	68,24517629	52,67902238	56,73	0,41%	32,13333224	4	-0,003176089	
	1	Z1	682,83	655,18	15	0,001178816	68,27875325	50,6696405	50,37	21,50%	6,975759839	0	-0,009800198	
D2B5	1	X2	682,83	677,59	31	0,000712077	75,8260328	53,07434394	54,35	10,61%	0,369692411	1	-0,032332676	
	1	Y2	682,83	685,12	10	-0,000353046	58,84550445	55,34784979	58,37	8,21%	10,70725184	3	-0,001648215	
	1	Z2	682,83	655,55	36	0,00031116	75,30112754	54,16308066	52,42	43,29%	3,508673843	-2	0,0009255	
B4B5	1	X3	682,83	670,4	7	-0,000694125	46,55816473	48,04158599	54,49	3,79%	16,53247037	6	0,021657009	
	1	Y3	682,83	673,61	3	-0,000287224	46,18491916	48,36889941	57,54	0,31%	39,60600724	9	0,003929886	
	1	Z3	682,83	644,14	21	-0,001124962	93,30261315	46,93672246	49,51	26,37%	23,26328354	3	0,021007762	
F7B5	2	X1	691,47	669,47	12	-0,0014626	64,61722091	52,74705518	57,05	11,34%	12,95557628	4	0,008465943	
	2	Y1	691,47	672,75	5	-0,000633689	65,79306878	53,93924397	57,69	6,10%	24,12297473	4	0,008407393	
	2	Z1	691,47	646,00	14	0,003885157	85,27567399	53,98913571	50,96	30,14%	12,72895788	-3	-0,02556916	
C2B6	2	X2	691,47	682,11	7	-0,000459798	54,02957411	54,58497946	56,47	2,89%	7,356501832	2	0,006448813	
	2	Y2	691,47	688,55	13	-0,000539144	55,59567636	53,96957958	57,38	16,39%	13,90243557	3	0,005815399	
	2	Z2	691,47	663,59	2	-0,002738105	16,47242622	50,58542002	50,26	19,70%	4,117406652	0	-0,054322026	
D8B7	2	X3	691,47	664,92	22	-0,000985905	43,01311634	49,27258383	57,69	10,68%	26,61820562	8	0,006559372	
	2	Y3	691,47	665,12	12	0,000746996	49,82299076	47,28745867	56,24	1,66%	15,12374449	9	0,000946426	
	2	Z3	691,47	638,82	29	-0,000862838	55,11749667	44,47084518	48,27	35,78%	32,38507686	4	0,01349411	
C6B7	3	X1	682,2	674,68	6	-0,000519397	66,39864791	53,40707909	58,54	5,11%	7,198881184	5	0,010961118	
	3	Y1	682,2	675,77	7	-0,001632272	59,02708703	47,07461925	55,22	1,03%	30,27473802	8	-0,017426068	
	3	Z1	682,2	646,18	5	-0,004305372	52,6709827	48,13298245	51,91	21,93%	4,196970557	4	0,008652928	
C3B7	3	X2	682,2	685,00	3	0,000613703	59,70146414	51,70717744	53,52	7,78%	2,36418112	2	0,009078581	
	3	Y2	682,2	686,06	6	0,00190681	53,19546872	51,81292537	57,59	7,30%	6,731902555	6	-0,016878874	
	3	Z2	682,2	657,32	12	-0,002442603	49,63752966	51,16151977	56,75	2,14%	13,27494696	6	0,006376582	
D4C6?	3	X3	682,2	680	27	0,001373291	57,53084748	48,45223319	50		27,94980229	2	0,005114654	
	3	Y3	682,2	680	7	-0,004577637	68,08482819	50,86336693	50		7,016237882	-1	0,01754818	
	3	Z3	682,2	680	15	-0,001678467	54,51484696	51,92988447	50		14,52357409	-2	0,007681912	
E7B8	4	X1	649,952	666,46	7	-0,002757917	61,10655658	52,05796009	54,63	6,81%	7,925054482	3	0,008595785	
	4	Y1	649,952	669,93	4	-0,001932199	52,12903064	51,99874322	55,05	4,39%	22,58726634	3	0,005556912	
	4	Z1	649,952	635,44	29	-0,003054374	46,6215219	51,36179878	48,17	15,58%	26,34283734	-3	0,003506809	
	4	X2	649,952	670,75	103	0	0		53,12	2,70%			0	

Figure 62: Summary of both tests using the new MEMS. First part.

D2B8	4	Y2	649,952	682,11	8	0,00165687	50,47214788	52,46788541	55,86	6,59%	8,72991252	3	0,006025526
	4	Z2	649,952	654,31	0	-0,003422351	55,15268731	53,41042636	53,61	25,33%	0,376265211	0	0,005908881
	4	X3	649,952	683,68	11	-0,001348379	52,83713433	45,98871568	54,02	21,93%	12,78336623	8	0,001344457
A7B5	4	Y3	649,952	694,04	19	0,00017177	37,86115131	49,05440905	56,61	2,64%	21,61433878	8	0,002295764
	4	Z3	649,952	668,75	29	-0,001622788	50,02122192	47,00934801	49,48	7,05%	30,48915705	2	0,001691305
	5	X1	682,38	670,56	9	-0,001340905	59,15597575	51,92017906	54,42	10,14%	9,399107993	2	-0,032861208
E2B6	5	Y1	682,38	672,20	12	-0,003158507	51,80400322	53,65077919	57,64	4,84%	32,13584604	4	0,007825545
	5	Z1	682,38	648,98	5	-0,001054663	47,70642252	52,54175956	53,76	31,15%	4,236121063	1	-0,030668969
	5	X2	682,38	680,27	6	0,000269412	50,7104203	54,33665687	55,30	12,36%	5,26727728	1	-0,001242843
D3B6	5	Y2	682,38	682,48	11	0,001023333	68,50490149	53,08412913	55,97	10,30%	11,92067698	3	0,007769057
	5	Z2	682,38	656,36	5	-0,001166903	44,66199253	54,69535476	54,63	30,15%	5,178757075	0	-0,050639194
	5	X3	682,38	683,53	25	-0,001448944	51,22489524	51,49665747	55,60	2,99%	26,59445605	4	0,01222011
D1B8	5	Y3	682,38	687,64	23	-0,001730184	46,42971831	49,61584226	59,39	3,05%	26,9667552	10	-0,001627895
	5	Z3	682,38	659,63	20	-0,00162105	56,7525523	46,21890586	50,22	16,28%	21,60739739	4	0,028516497
	6	X1	689,58	674,32	9	-0,002938116	52,28231637	54,18768652	56,71	9,44%	9,335365635	3	0,005746737
B5B5	6	Y1	689,58	675,24	5	-0,000319708	46,80544869	55,92821966	55,67	3,98%	23,64413219	0	0,001440985
	6	Z1	689,58	648,55	8	-0,002278646	46,76295173	52,85832459	49,98	41,88%	6,724860757	-3	-0,03544589
	6	X2	689,58	688,49	4	-0,00195545	52,8454208	53,45706262	58,01	3,44%	4,199853459	5	0,003310325
D1B5	6	Y2	689,58	690,65	12	0,000286284	73,14144543	55,88742719	58,55	10,66%	12,77586151	3	0,00826527
	6	Z2	689,58	664,76	1	-0,003764997	48,65987964	53,67021206	53,67	10,01%	0,852231668	0	-0,04335882
	6	X3	689,58	671,88	40	-8,55018E-06	47,57750216	46,85650631	57,12	4,09%	49,04499373	10	-0,00210275
D7B7	6	Y3	689,58	673,94	5	-0,002922409	41,4842655	50,64421023	58,23	2,72%	5,261501511	8	0,002046747
	6	Z3	689,58	643,76	14	0,000922324	41,89713619	51,25545191	52,90	20,47%	14,74103424	2	0,040286247
	7	X1	671,436	666,34	13	-0,003464903	64,70950921	50,74066793	54,03	14,14%	13,72439188	3	0,007388605
E8B7	7	Y1	671,436	666,63	0	-0,001263849	62,26242856	55,89627086	55,72	1,07%	18,23700435	0	-0,032021197
	7	Z1	671,436	640,84	16	-0,003059966	56,25974549	52,17042455	52,71	29,86%	15,05567492	1	0,006162995
	7	X2	671,436	670	2	0,00032557	68,41190632	51,94562264	50		1,170408249	-2	0,003998162
C7B7?	7	Y2	671,436	670	1	-0,002472966	52,67415353	53,91278638	50		0,769057207	-4	-0,01208915
	7	Z2	671,436	670	24	-0,003764827	39,88814311	51,52120769	50		23,22673287	-2	0,006376259
	7	X3	671,436	666,86	24	-0,002219087	44,29652201	47,2548543	54,13	13,55%	27,00258924	7	0,002420498
E8B6	7	Y3	671,436	669,85	3	-0,000559284	57,72328464	45,94212352	54,26	20,63%	3,577047328	8	0,020739227
	7	Z3	671,436	642,07	25	-0,002828413	51,26896402	50,83177259	55,17	31,75%	27,60883848	4	0,000256348
	8	X1	675,108	673,91	24	-0,00050354	52,49019692	52,43892921	54,88	23,15%	24,86347032	2	0,00655438

Figure 63: Summary of both tests using the new MEMS. Second part.

B8B2	8	Y1	675,108	679,36	3	0,003095354	45,07686572	52,92632652	53,97	9,50%	23,14797738	1	0,008316173	
	8	Z1	675,108	661,64	9	-0,000584194	48,22029749	50,99900005	67,46	0,93%	10,47118837	16	-0,004298467	Split3B
E8B5	8	X2	675,108	666,47	11	0,000306532	51,71025186	52,5789327	56,18	1,24%	10,96530911	4	0,003759766	
	8	Y2	675,108	667,44	6	0,000606961	55,12092077	51,39760347	54,28	3,23%	6,413631103	3	0,003237782	
	8	Z2	675,108	641,59	3	-0,000739204	76,15043811	47,98458986	53,17	23,38%	3,245208436	5	-0,014241625	
E2B7	8	X3	675,108	669,97	9	-0,000377128	51,32248851	60,05945902	56,87	7,35%	8,244809064	-3	0,002437919	
	8	Y3	675,108	667,90	17	-0,000622137	52,39739543	49,85847941	56,05	5,96%	19,21013261	6	0,001837283	
	8	Z3	675,108	644,39	27	0,001141153	55,99806226	51,58724767	51,67	33,18%	27,13802446	0	0,009274603	
F8B7	9	X1	681,75	673,39	3	-0,000532709	68,70242354	53,72067354	55,70	2,69%	3,690750202	2	0,013077343	
	9	Y1	681,75	675,75	9	-0,003723003	98,29311939	50,62887676	54,86	9,53%	30,24898079	4	0,001716707	
	9	Z1	681,75	650,66	9	0,000556555	53,606702	51,94966856	48,94	30,25%	7,997675462	-3	0,007630204	
F2B5	9	X2	681,75	674,13	12	-0,003023035	72,31789653	52,16554155	53,99	6,88%	11,634188	2	0,01327689	
	9	Y2	681,75	679,96	10	-0,001436121	57,29054083	53,13223007	57,13	6,88%	10,18251074	4	-0,002107083	
	9	Z2	681,75	652,19	15	-0,003867834	55,08887121	52,56128406	53,66	47,12%	14,56004075	1	-0,06235227	
C8B8	9	X3	681,75	674,99	24	-0,000709025	48,57369326	47,27266791	54,07	5,16%	26,94963159	7	0,000726449	
	9	Y3	681,75	677,68	38	2,84831E-05	52,78929095	49,37854185	55,99	11,21%	42,88814086	7	0,002190207	
	9	Z3	681,75	651,85	10	-0,001110331	36,51749801	44,72139057	47,74	5,74%	10,45553165	3	0,002542972	
E3B6	10	X1	644,85	677,87	4	-0,002050283	56,86458491	52,87674568	54,74	2,33%	3,870934478	2	0,006603449	
	10	Y1	644,85	680,57	7	-0,004087113	56,72572146	50,52327418	57,96	10,28%	29,17496678	7	-0,002986284	
	10	Z1	644,85	652,80	14	-0,003901517	67,62805774	53,60751109	53,99	20,67%	13,06800839	0	0,01274858	
D6B6	10	X2	644,85	673,69	13	0,000267877	58,88545527	54,92587619	53,81	4,72%	11,97805737	-1	0,018018133	
	10	Y2	644,85	681,00	18	-0,000354343	61,99961546	52,21118846	55,71	16,12%	18,75455862	4	-0,011841375	
	10	Z2	644,85	649,79	11	-0,00269911	56,33165265	50,67542541	58,42	27,47%	11,95313163	8	-0,069480757	
D6B7	10	X3	644,85	677,97	113	0	0	#DIV/0!	55,23	9,66%	#DIV/0!		#DIV/0!	
	10	Y3	644,85	684,34	22	-0,000585918	14,3102646	51,41140855	56,01	8,82%	23,84628488	5	0,000782606	
	10	Z3	644,85	649,48	16	3,06613E-05	24,7848207	50,88808333	57,43	21,83%	17,91931501	7	0,001535373	
			675,1556									4		
				< 700 Ohm	=< 30 %		|40| < val< |60|	|40| < val< |60|	|40| < val< |60|	=< 30 %	=< 30 %	-10 < val< 10		
				< 1000 Ohm	=< 50 %		|30| < val< |65|	|30| < val< |65|	|30| < val< |65|	=< 50 %	=< 50 %	-15 < val< 15		
				> 1000 Ohm	=> 50 %			Out of limit	Out of limit			Out of limit		

Figure 64: Summary of both tests using the new MEMS. Third part. The split 3B corresponds to another design for the self test axis on Z that wasn't chosen in the future because of complications during the microfabrication. This axis has not been plotted in any figure of the report.